Original Article

MOLECULAR METABOLISM

Skeletal muscle O-GlcNAc transferase is important for muscle energy homeostasis and whole-body insulin sensitivity

Hao Shi [1,11], Alexander Munk [2,11], Thomas S. Nielsen [2], Morgan R. Daughtry [1], Louise Larsson [2], Shize Li [1], Kasper F. Høyer [2,3], Hannah W. Geisler [1], Karolina Sulek [2], Rasmus Kjøbsted [4], Taylor Fisher [1], Marianne M. Andersen [2], Zhengxing Shen [1], Ulrik K. Hansen [2], Eric M. England [1], Zhiyong Cheng [5], Kurt Højlund [6,7], Jørgen F.P. Wojtaszewski [4], Xiaoyong Yang [8], Matthew W. Hulver [5,9], Richard F. Helm [10], Jonas T. Treebak [2,*], David E. Gerrard [1,]**

ABSTRACT

Objective: Given that cellular O-GlcNAcylation levels are thought to be real-time measures of cellular nutrient status and dysregulated O-GlcNAc signaling is associated with insulin resistance, we evaluated the role of O-GlcNAc transferase (OGT), the enzyme that mediates O-GlcNAcylation, in skeletal muscle.

Methods: We assessed O-GlcNAcylation levels in skeletal muscle from obese, type 2 diabetic people, and we characterized muscle-specific OGT knockout (mKO) mice in metabolic cages and measured energy expenditure and substrate utilization pattern using indirect calorimetry. Whole body insulin sensitivity was assessed using the hyperinsulinemic euglycemic clamp technique and tissue-specific glucose uptake was subsequently evaluated. Tissues were used for histology, qPCR, Western blot, co-immunoprecipitation, and chromatin immunoprecipitation analyses.

Results: We found elevated levels of O-GlcNAc-modified proteins in obese, type 2 diabetic people compared with well-matched obese and lean controls. Muscle-specific OGT knockout mice were lean, and whole body energy expenditure and insulin sensitivity were increased in these mice, consistent with enhanced glucose uptake and elevated glycolytic enzyme activities in skeletal muscle. Moreover, enhanced glucose uptake was also observed in white adipose tissue that was browner than that of WT mice. Interestingly, mKO mice had elevated mRNA levels of *Il15* in skeletal muscle and increased circulating IL-15 levels. We found that OGT in muscle mediates transcriptional repression of *Il15* by O-GlcNAcylating Enhancer of Zeste Homolog 2 (EZH2).

Conclusions: Elevated muscle O-GlcNAc levels paralleled insulin resistance and type 2 diabetes in humans. Moreover, OGT-mediated signaling is necessary for proper skeletal muscle metabolism and whole-body energy homeostasis, and our data highlight O-GlcNAcylation as a potential target for ameliorating metabolic disorders.

Keywords O-GlcNAc signaling; Type 2 diabetes; N-acetyl-D-glucosamine; Tissue cross talk; Epigenetic regulation of *Il15* transcription; Insulin sensitivity

1. INTRODUCTION

Protein modification by O-linked β-D-N-acetylglucosamine (O-GlcNAc) is a post-translational event that results in the transfer of a sugar derivative emanating from the hexosamine biosynthetic pathway to a variety of cellular proteins [1]. Several lines of evidence support the notion that the addition and removal of an O-GlcNAc moiety from serine and threonine hydroxyls by O-GlcNAc transferase (OGT) and O-

[1]Department of Animal and Poultry Sciences, Virginia Polytechnic Institute and State University, Blacksburg, VA 24061, USA [2]Section of Integrative Physiology, Novo Nordisk Foundation Center for Basic Metabolic Research, Faculty of Health and Medical Sciences, University of Copenhagen, Copenhagen, DK2200, Denmark [3]Department of Endocrinology and Internal Medicine, Aarhus University Hospital, Aarhus, DK8000, Denmark [4]Section of Molecular Physiology, Department of Nutrition, Exercise and Sports, Faculty of Science, University of Copenhagen, Copenhagen, DK2100, Denmark [5]Department of Human Nutrition, Foods, and Exercise, Virginia Polytechnic Institute and State University, Blacksburg, VA 24061, USA [6]Department of Endocrinology, Odense University Hospital, Odense, Denmark [7]Section of Molecular Diabetes and Metabolism, Institute of Molecular Medicine and Institute of Clinical Research, University of Southern Denmark, Odense, Denmark [8]Department of Cellular and Molecular Physiology, Yale University School of Medicine, New Haven, CT 06520, USA [9]The Virginia Tech Metabolic Phenotyping Core, Blacksburg, VA 24061, USA [10]Department of Biochemistry, Virginia Polytechnic Institute and State University, Blacksburg, VA 24061, USA

[11] These authors contributed equally.

*Corresponding author. E-mail: jttreebak@sund.ku.dk (J.T. Treebak).

**Corresponding author. E-mail: dgerrard@vt.edu (D.E. Gerrard).

Received January 18, 2018 • Revision received February 18, 2018 • Accepted February 19, 2018 • Available online 24 February 2018

https://doi.org/10.1016/j.molmet.2018.02.010

GlcNAcase (OGA), respectively, serve as an integrated cellular nutrient sensor. First, the amount of O-GlcNAc-modified cellular proteins increases in response to elevated nutrient and energy availabilities [2]. Second, the activity of key signaling molecules in the canonical insulin signaling pathway, such as the β subunit of the insulin receptor, IRS1, IRS2, p85 and p110 subunits of PI3K, PDK1, and Akt is generally inhibited by OGT-dependent O-GlcNAcylation [3–7]. Third, transcription co-factors such as FOXO1 and PGC-1α, which are master regulators of gluconeogenesis and lipid metabolism, respectively, are targeted by OGT which results in the stabilization of the proteins [8]. Fourth, OGT and the energy sensor AMP-activated protein kinase (AMPK) physically interact and mutually modify each other's function and/or localization [6,9]. Accordingly, dysregulation of cellular O-GlcNAcylation may be involved in the pathogenesis of a number of metabolic diseases, including obesity and type 2 diabetes [10,11]. This is evidenced by findings showing critical roles of O-GlcNAcylation status in AgRP and α-CaMKII positive neurons for maintaining whole body energy balance in mice [12,13].

Skeletal muscle is an important metabolic tissue and plays essential roles in locomotion and thermogenesis, both having significant impacts on global glucose metabolism and insulin sensitivity [14–17]. Skeletal muscle utilizes a highly complex set of intercalated and coordinated signaling mechanisms to respond to altered environmental nutritional cues [18–20]. Previous studies have suggested that dysregulated O-GlcNAc signaling in skeletal muscle is associated with the development of several metabolic diseases. For example, over-expression of OGT in muscle and adipose tissue causes insulin resistance and impairs glucose transport, respectively [21,22]. In addition, over-expression of OGA, which eliminates O-GlcNAcylation, impairs myogenesis and induces muscle atrophy [23,24]. These findings suggest that O-GlcNAcylation may be part of a complex signaling mechanism within skeletal muscle that is responsible for monitoring cellular nutrient availability and conveying this information to downstream targets to induce metabolic adaptation. Apart from the studies mentioned above, however, the precise role of O-GlcNAcylation in skeletal muscle remains largely unexplored. Herein, we show that skeletal muscle from type 2 diabetic humans has elevated O-GlcNAcylation levels compared with matched controls. Moreover, we show that knockout of OGT in skeletal muscle in mice causes alterations of muscle metabolism that improves whole-body insulin sensitivity and increases energy expenditure. We propose a mechanism whereby lack of OGT results in perturbed regulation of *Il15* expression, which subsequently drives the observed phenotype.

2. MATERIALS AND METHODS

2.1. Human samples

Human skeletal muscle samples were obtained from a previous study [25]. In short, muscle samples were obtained from the vastus lateralis muscle (Bergström needle biopsy) before and after a 4-hour euglycemic hyperinsulinemic clamp (40 mU * m^{-2} * min^{-1}) under local anesthesia. Muscle biopsy samples were quickly blotted free of blood and frozen in liquid nitrogen. Muscle lysates were prepared from freeze-dried muscle dissected free of visible blood, fat, and connective tissue and homogenized as previously described [26]. Lysates were collected from the supernatant of homogenates centrifuged for 20 min at 16,000 *g* and 4 °C. Total protein content in lysates was analyzed by the bicinchoninic acid method (ThermoFisher Scientific). Muscle lysates were prepared in Laemmli buffer and heated for 10 min at 96 °C after which equal amounts of protein were separated by SDS-PAGE. Proteins were transferred to PVDF membranes and incubated with the indicated antibodies.

2.2. Animals

Mice were generated and experiments performed at either the Novo Nordisk Foundation Center for Basic Metabolic Research, University of Copenhagen, or Virginia Polytechnic Institute and State University. Muscle specific *Ogt* deletion was achieved by breeding $HSA^{Cre/+}$;$Ogt^{LoxP/Y}$ (JaxMice, strain: B6.Cg-Tg(ACTA1-cre)79Jme/J) males with $Ogt^{LoxP/LoxP}$ females to generate $HSA^{+/+}$;$Ogt^{LoxP/Y}$ (WT) and $HSA^{Cre/+}$;$Ogt^{LoxP/Y}$ (mKO) mice. Inducible muscle-specific OGT knockout mice were generated by breeding HSA-rtTA/TRE-Cre (JaxMice, strain B6;C3-Tg(ACTA1-rtTA,tetO-Cre)102Monk/J) male mice with $Ogt^{LoxP/LoxP}$ females. All procedures were approved by the Danish Animal Experiments Inspectorate and complied with the European convention for protection of vertebrate animals used for scientific purposes (EU Directive 2010/63/EU for animal experiments), or they were approved by Institutional Animal Care and Use Committee of the Virginia Polytechnic Institute and State University and complied with the National Institutes of Health guidelines (NIH Publications No. 8023). Mice were group-housed in an enriched environment with a 12 h light:12 h dark cycle with *ad libitum* feed (#1310, Altromin for mice at University of Copenhagen, and #2918, Envigo for mice at Virginia Polytechnic Institute and State University) and water in a temperature-controlled (22 °C ± 1 °C) room. Mice used for HFD study were fed Teklad rodent diets (#TD.06414, Envigo) with 60% calories coming from fat. The fatty acid profile (% of total fat) is as follows: 37% saturated, 47% monounsaturated, 16% polyunsaturated. The control diet was the standard chow (#2918, Envigo). Mice were fed HFD or normal chow from 4 weeks of age for the indicated weeks.

2.3. Whole body metabolic assessment

Whole body metabolic phenotyping was performed at Virginia Tech Metabolic Phenotyping Core using the TSE LabMaster Indirect Calorimetry System. For acclimation purpose, mice were housed in a mock LabMaster cage for one week before they were transferred to recording cages to measure locomotor activity and indirect calorimetry. Mice were fed *ad libitum* during the indicated experimental period. Cage activity, energy expenditure normalized to lean body mass, and respiratory exchange rates were recorded for a 48-h period at the interval of 20 min. Whole body composition was measured by MRI (Minispec Whole Body Composition Analyzer, Bruker). Rectal temperature was recorded at 4PM using an ETI Microtherma 2 Type T thermometer (ThermoWorks). The probe was inserted into the anal ducts of the mice (around 2 cm) when animal was awake in the absence of anesthesia.

2.4. Histology and immunohistochemistry

Muscle, WAT, liver, and pancreas were collected from WT and mKO mice and fixed in 10% neutral buffered formalin (0.4% sodium phosphate monobasic, 0.65% sodium phosphate dibasic, 10% formalin, pH 6.8) overnight. The tissues were then washed twice in 70% ethanol, and paraffin-embedded. For H&E staining, tissue sections were de-paraffinized with two exchanges of xylene, rehydrated in 100%, 95%, and 70% ethanol respectively. After a brief wash in water, sections were stained in Harris hematoxylin for 8 min, washed in running water for 1 min, soaked in 0.2% ammonia water for 1 min. After washing in running water for 5 min, the tissue sections were rinsed in 95% ethanol for 10 s. Sections were then counterstained with eosin solution for 30 s, dehydrated in 95% ethanol, 100% ethanol, and

xylene, and mounted for microscopy. For immunohistochemical staining, paraffin-embedded sections were de-paraffinized and re-hydrated, and antigen was retrieved by heating the sections in boiling sodium citrate buffer (10 mM sodium citrate, 0.05% Tween 20, pH 6.0) for 30 min. After cooling down at room temperature for 20 min, tissue sections were blocked in 5% goat serum for 1 h at room temperature before applying primary antibodies anti-UCP1 (#10983 Abcam) or anti-succinate dehydrogenase (#14715 Abcam), 1:200 diluted in 5% goat serum. After incubation in the primary antibody overnight at 4 °C, sections were washed in 1 x PBS three times with 5 min each. The sections were then incubated in Alexa Fluor 488 conjugated goat anti rabbit IgG (#A-11078 ThermoFisher Scientific) or Alexa Fluor 555 goat anti mouse IgG (#A-21424 ThermoFisher Scientific) highly cross-absorbed antibodies, respectively, for 1 h at room temperature, washed in PBS, and mounted in fluorescent mounting medium for microscopy. Images were taken using a Nikon ECLIPSE Ti-E fluorescent microscope (Nikon Instruments).

2.5. *Ex vivo* EDL and soleus muscle contractility assay

Isolated soleus and extensor digitorum longus (EDL) muscles from male mice (12–16 weeks of age) were used for muscle contractility assays. Muscles were incubated at 30 °C in oxygenated (95% O2 and 5% CO2) physiological salt solution as previously described in [27] for Figure 1M–P and in [28] for Figure 1Q–T. The buffer was continuously oxygenated with 95% O2 and 5% CO2 during the incubation period and maintained at 30 °C. For results shown in Figure 1M–P, muscles were set to an initial resting tension of 10 mN (optimal length, L0; 300B, Aurora Scientific) and maintained by a stepper motor. Dynamic Muscle Control software (DMC Version 4.1.6, Aurora Scientific) was used to control the force and position inputs of the servomotor arm and the stepper motor. For results shown in Figure 1M–O, the stimulated muscle was subjected to 3 isometric twitches and two tetani (150 Hz) each separated by 1 min. For Figure 1P, the muscle was subjected to a force frequency protocol consisting of 6 stimulations of increasing frequency (1, 30, 50, 80, 100, and 150 Hz), one min apart. For results shown in Figure 1Q–T, muscles were incubated in a muscle strip myograph system (820MS, DMT, Denmark) at a 5–6 mN tension. Muscles were stimulated to contract using the following protocol: stimulus frequency 100 Hz; stimulus width 0.2 ms; stimulus train duration 1 sec train every 15 sec. The total stimulation protocol was 9 min.

2.6. Hyperinsulinemic euglycemic clamp experiments

The hyperinsulinemic euglycemic clamp was performed in conscious, unrestrained male mice at 17–19 weeks of age as previously described [29]. For the surgical catheterization, mice were anesthetized with isoflurane (2.5% for induction, 1.5% for maintenance). Lidocain (7 mg/kg; Xylocain, AstraZeneca, Sweden) and Carprofen (10 mg/kg; Rimadyl, Pfizer, USA) were administered preoperatively for analgesia. All surgical procedures were conducted using strictly aseptic techniques. The carotid artery and jugular vein were cannulated and the catheters were externalized on the back (caudal to the scapulae) with a dual channel vascular access button (Instech, PA, USA). After surgery, the catheters were locked with heparinized saline (200 U/mL) and the animals recovered for 6–7 days. Body weight was recorded before and 24 h after the operation and on the day of the clamp. The inclusion criteria following surgery were a weight loss of less than 10% and a hematocrit above 35% by day 6–7. All mice fulfilled these criteria. On the day of the clamp experiment, mice were fasted for 5 h starting at 7:30 AM ($t = -300$ min) by placing them in a clean cage with bedding and nesting material, and free access to water. At $t = -120$ min the mice were placed in a new cage of ~20 × 20 cm, the catheters were flushed with heparinized saline (10 U/mL) and the mice were connected to the infusion lines. A tracer equilibration period was started at $t = -90$ min by infusion of a 1.2 μCi priming dose of [3-3H]glucose (Product no. NET331C005 MC; Perkin Elmer, USA) followed by a constant 0.04 μCi/min infusion of [3-3H]glucose for 90 min. Blood samples were collected for the assessment of baseline hematocrit level (40 μL) as well as basal glucose levels and turnover rates at $t = -15$ min (50 μL) and −5 min (100 μL), respectively. The clamp was initiated at $t = 0$ min with continuous infusions of human insulin (4 mU/kg/min; Actrapid, Novo Nordisk, Denmark) and washed red blood cells obtained from a donor mouse to compensate for the blood loss due to repeated sampling (5 μL/min of 50% RBC in 10 U/ml heparinized saline). Blood glucose was measured every 10 min (Contour XT; Bayer, USA) and euglycemia was maintained by adjusting a variable infusion of 50% glucose containing 0.06 μCi/μL of [3-3H]glucose tracer. Between $t = 80$ and $t = 120$ min blood samples (50–100 μL) were collected in 10 min intervals and processed for determination of [3-3H]glucose specific activity. At $t = 110$ min hematocrit was measured again to ensure that hematocrit levels were stable. At $t = 120$ min a 12 μCi bolus of 2-[1–14C]-deoxy-D-glucose (Product no. NEC495250UC; Perkin Elmer, USA) was injected and blood samples were collected at $t = 122$, 125, 135, 145, and 155 min, respectively. These samples were processed for determination of 2-[1–14C]-deoxy-D-glucose specific activity. After the final blood sample, mice were euthanized with a lethal dose of pentobarbital and tissues were collected and snap-frozen in liquid nitrogen. The tissues were processed for determination of 2-[1–14C]-deoxy-D-glucose specific activity in order to calculate tissue-specific glucose uptake.

2.7. Clamp sample processing and calculations

Plasma samples were deproteinized with $Ba(OH)_2$ and $ZnSO_4$, and aliquots of each supernatant were transferred to 2 scintillation vials. To determine plasma [3-3H]glucose, one of the aliquots was dried and resuspended in MilliQ water to remove $3H_2O$ and the other was counted directly (Hidex 300 SL). Supernatants for 2-[1–14C]-deoxy-D-glucose determinations were counted directly. Total plasma glucose concentration was determined by adding a reaction mix (200 mM Tris–HCl, 500 mM MgCl2, 5.2 mM ATP, 2.8 mM NADP, and 148 μg of a hexokinase and G6PDH mixture (Roche, Germany) pH 7.4) to each sample and measuring absorbance at 340 nm. Parameters related to glucose turnover rates (Ra, Rd, endoRa, glycolysis) were calculated as previously described [30]. Tissues were homogenized in ice-cold lysis buffer (pH 7.4, 10% glycerol, 1% IGEPAL, 50 mM Hepes, 150 mM NaCl, 10 mM NaF, 1 mM EDTA, 1 mM EGTA, 20 mM sodium pyrophosphate, 2 mM sodium orthovanadate, 1 mM sodium-pyrophosphate, 5 mM nicotinamide, 4 μM Thiamet G, and protease inhibitors (SigmaFast)). Aliquots of each crude homogenate were transferred to two 1.5 mL tubes and deproteinized with 4.5% perchloric acid or $Ba(OH)_2 + ZnSO_4$. Supernatants were transferred to scintillation vials and counted to determine 2-[1–14C]-deoxy-D-glucose content. Tissue-specific glucose uptake rates were calculated as described previously [31].

2.8. Insulin and glucose tolerance test

Mice were fasted for four hours before insulin tolerance test (ITT). Bovine insulin (Sigma) was prepared in sterile saline and intraperitoneally injected at the dosage of 1 U/kg body weight. Blood glucose level was measured at 0, 15, 30, 60, 90, and 120 min after insulin injection using OneTouch Ultra2 test strip and glucometer. For

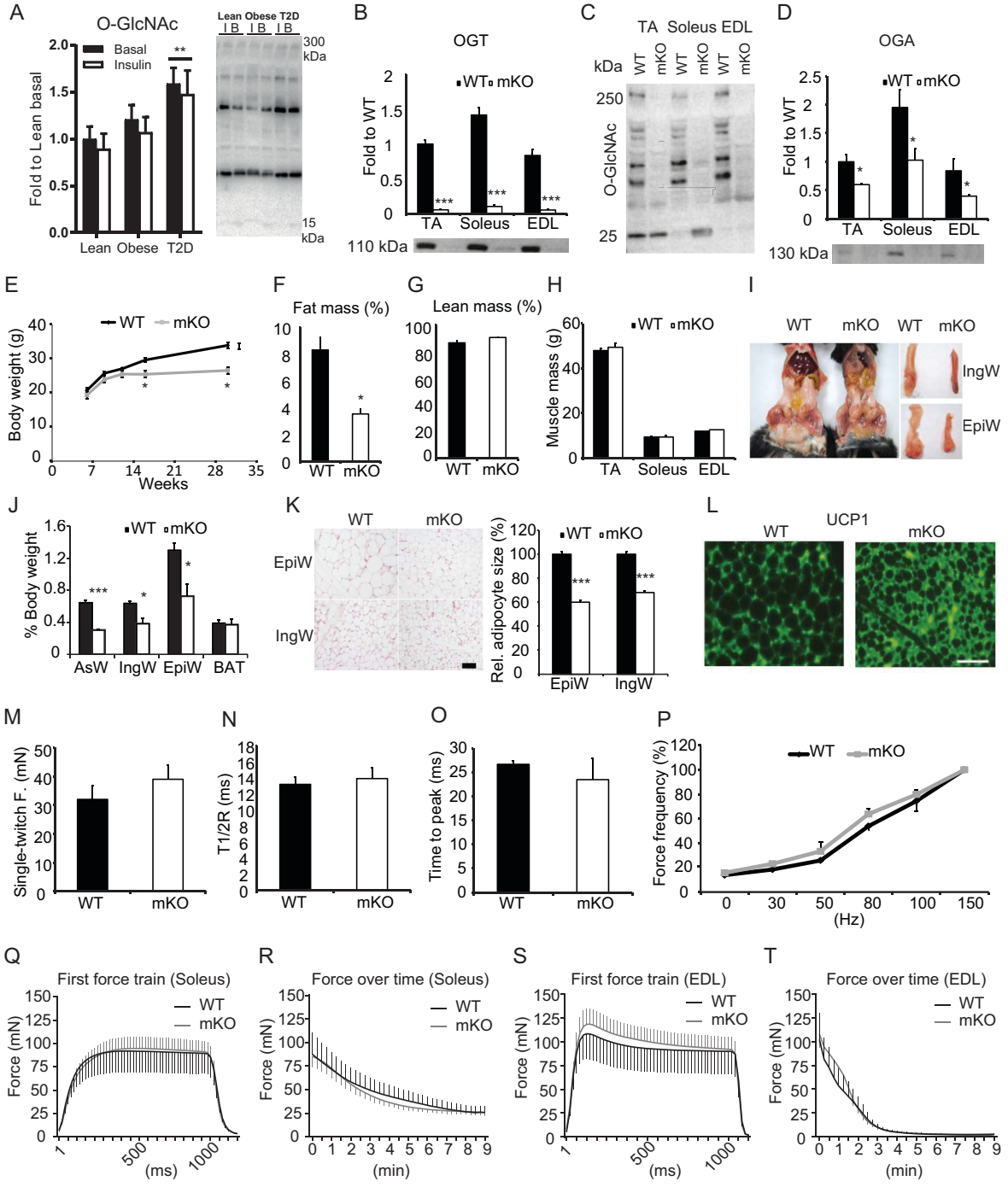

Figure 1: Mice lacking OGT in skeletal muscle exhibit reduced fat mass but normal skeletal muscle morphology and contractility. (A) O-GlcNAc levels in human skeletal muscles of lean, obese, and type 2 diabetic individuals at basal (B) and after a hyperinsulinemic euglycemic clamp (Insulin (I)). Lane intensities were quantified between 15 and 300 kDa. Sample size of 8–10 people per group. Data are mean ± SEM and analyzed by two-way repeated measures ANOVA; ** indicates $p < 0.01$. **(B)** OGT, **(C)** O-GlcNAc, and **(D)** OGA immunoblotted in tibialis anterior (TA), soleus, and extensor digitorum longus (EDL) muscles from WT and mKO mice (n = 4). **(E)** Body weights of WT and mKO mice measured at 6, 9, 12, 16, and 30 weeks of age (n = 6–10). **(F–H)** Body composition: fat percentage (F), lean percentage (G), and muscle weights (H) of TA, soleus, and EDL in 16-week-old WT and mKO mice (n = 10). **(I)** Images comparing abdominal, inguinal (lngW) and epididymal (EpiW) white adipose tissue (WAT) depots from WT and mKO mice. **(J)** Quantification of adipose tissue weights expressed as percentage (%) body weight (n = 10). **(K)** Representative micrographs of H&E stained sections from epididymal (EpiW) and inguinal (lngW) white adipose tissues (WAT) of WT and mKO mice. Scale bar, 100 μm. The relative size of adipocytes in the EpiW and lngW of mKO mice was expressed as a percentage of WT (n = 10). **(L)** Immunoreactive uncoupling protein 1 (UCP1) in lngW of WT (left) and mKO (right) mice. Scale bar, 100 μm. **(M–O)** EDL muscle single-twitch contraction force (M), time-to-half relaxation tension (T1/2R; n = 10) (N), and time to peak of tension (n = 10) (O). **(P)** EDL muscle contractile force in response to increased stimulation frequency (n = 10). Data normalized to force at 150 Hz. **(Q,R)** First force train at 100Hz, 1 sec duration in soleus (Q; n = 5), and fatigue-ability measured as force produced over consecutive force trains at 100 Hz, 1 sec duration in soleus (R; n = 5). **(S,T)** First force train at 100 Hz, 1 sec duration in EDL (S; n = 5), and fatigue-ability measured as force produced over consecutive force trains at 100 Hz, 1 sec duration in EDL (T; n = 5). Data in B-T are means ± SEM from 16-week-old male mice. *$p < 0.05$; **$p < 0.01$; ***$p < 0.001$ compared with WT mice.

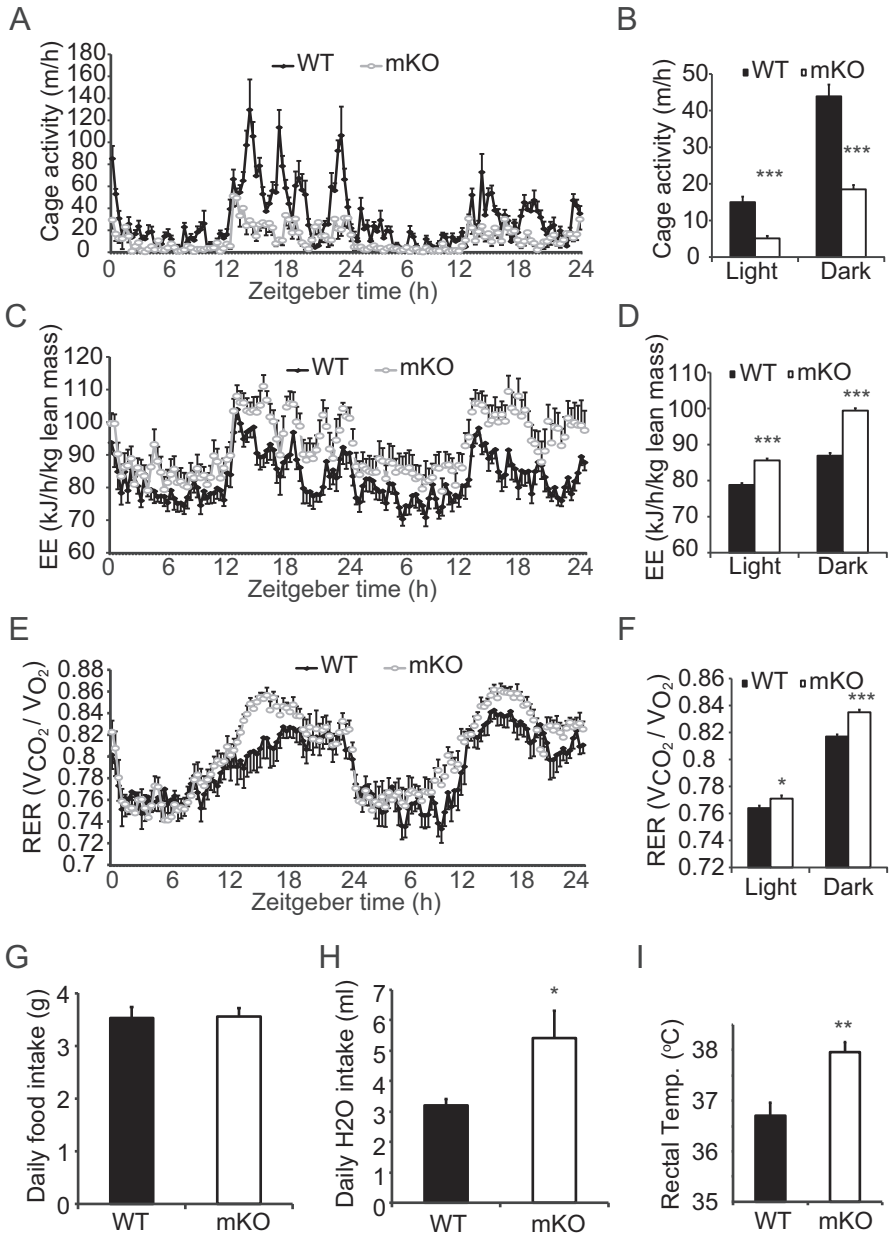

Figure 2: OGT mKO mice are less active and have higher whole body energy expenditure. (A–F) Cage activity (real-time, A, and tabular, B), energy expenditure per lean body mass (EE) (real-time, C, and tabular, D) and respiratory exchange ratio (RER) (real-time, E, and tabular, F) for WT and mKO mice (n = 10). Measurements were recorded every 20 min using TSE Lab-Master System. A, C, and E: X-axis represents zeitgeber time, with 0 at lights on. **(G–I)** Daily food intake (G) and water consumption (H), and rectal temperatures (I) for WT and mKO mice (n = 10). Data represent means ± SEM from 16-week-old male mice. *p < 0.05; **p < 0.01; ***p < 0.001 compared with WT mice.

glucose tolerance test (GTT), mice were fasted overnight (16 h) before the experiment, glucose was intraperitoneally injected at the dosage of 2 g/kg body weight, and blood collection and measurement were the same as ITT.

2.9. Skeletal muscle mitochondrial isolation

Isolation of mitochondria from skeletal muscle was performed as previously described [32]. Briefly, quadriceps femoris and gastrocnemius muscles were collected in buffer containing 67 mM sucrose, 50 mM Tris/HCl, 50 mM KCl, 10 mM EDTA/Tris, and 10% BSA (Sigma). Before homogenization, muscle samples were minced with scissors, and digested in PBS containing 0.05% trypsin (Invitrogen) and 10 mM EDTA (Sigma) for 30 min. Muscles were homogenized with a Teflon pestle at the speed of 1,600 rpm and mitochondria were isolated by differential centrifugation.

2.10. Respirometry of isolated mitochondria

Mitochondrial respiration was measured using an XF24 extracellular flux analyzer (Seahorse bioscience) as previously described [33]. Freshly isolated mitochondria were seeded at 5 μg per well in a Seahorse XF Cell Culture Microplate. Mitochondria were suspended in a sucrose/mannitol solution containing pyruvate (10 mM) and malate (5 mM). Mitochondria were mixed for 25 sec before the measurement cycles. Oxygen consumption rates (OCRs) at basal conditions (state 2),

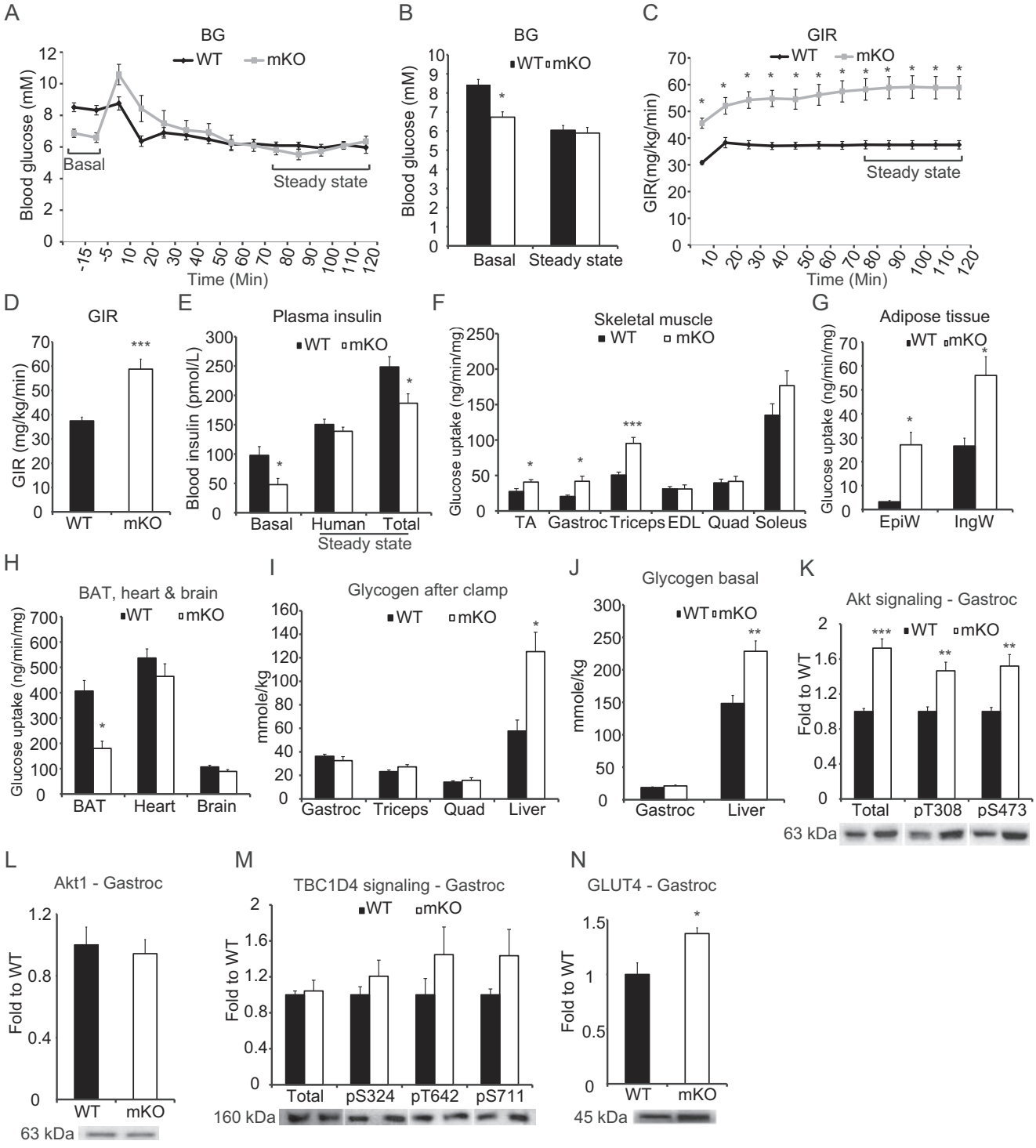

Figure 3: Lack of OGT in skeletal muscle affects glucose homeostasis and insulin signaling. (A–B) Blood glucose levels before and during a hyperinsulinemic euglycemic clamp performed using 4 mU/kg/min of insulin. **(C–D)** Glucose infusion rates (GIR) during clamp. **(E)** Plasma insulin levels before and during steady state of the clamp. **(F)** Glucose uptake in skeletal muscles after steady state. **(G)** Glucose uptake in adipose tissues after steady state. **(H)** Glucose uptake in BAT, heart, and brain after steady state. **(I)** Glycogen in gastrocnemius, triceps, quadriceps and liver from clamped mice. **(J)** Glycogen in gastrocnemius and liver from 5-hour fasted mice. **(K)** Immunoblot of Akt and Akt phosphorylation of pS473 and pT308 in gastrocnemius. **(L)** Immunoblot of Akt1 in gastrocnemius from clamped mice. **(M)** Immunoblot of TBC1D4 and TBC1D4 phosphorylation of, pS324, pT642, and pS711 in gastrocnemius. **(N)** Immunoblot of GLUT4 in gastrocnemius. Data represent means ± SEM from n = 8–10 mice in each genotype. Mice were 18-week-old males. *p < 0.05; **p < 0.01; ***p < 0.001 compared with WT mice.

ADP (5 mM) stimulation (state 3), ADP exhaustion (state 4), oligomycin (2 μM) induction (state 4°), and FCCP (0.3 μM) induction were measured to assess mitochondrial oxidative capacity. All experiments were performed at 37 °C.

2.11. Fatty acid oxidation and PDH activity assay

Fatty acid oxidation was assessed in muscle homogenates as previously described [34]. Briefly, [1−^{14}C]-palmitic acid (Perkin Elmer) was used as the substrate, $^{14}CO_2$ production and ^{14}C-labeled acid-soluble metabolites were measured by liquid scintillation counting. Pyruvate dehydrogenase (PDH) activity was assayed using [1−^{14}C]-pyruvate as substrate, enzyme catalyzed release of $^{14}CO_2$ was counted to reflect PDH enzyme activity.

2.12. Citrate synthase (CS) and malate dehydrogenase (MDH) activity assay

CS and MDH activities were determined as previously described [34]. CS activity was determined by the rate of DNTB reduction upon exposure to acetyl CoA, the product (TNB) is measured spectrophotometrically at 412 nm. Malate dehydrogenase (MDH) activity was determined by the rate of NADH oxidation in the presence of oxaloacetate and measured at 340 nm.

2.13. Western blot analyses

Skeletal muscle samples used in Figures 7 and 8 were lysed in RIPA buffer (in mM: 200 NaCl, 20 Tris-Cl at pH 8.0, 1 EDTA, 1 EGTA, 1% Nonidet P-40, 0.5% sodium deoxycholate, 0.1% SDS, 2.5 sodium pyrophosphate, 1 β-glycerol phosphate, 1 Na_3VO_4, and protease inhibitor cocktail (Sigma) and protein concentration was determined using a Bicinchoninic Acid (BCA) Protein Assay kit (Pierce). All other tissue samples were processed using steel bead homogenization (Tissue Lyser II, Qiagen) in ice-cold lysis buffer (pH 7.4; 10% glycerol; 1% IGEPAL; Hepes, 50 mM; NaCl, 150 mM; NaF, 10 mM; EDTA, 1 mM; EGTA, 1 mM; sodium pyrophosphate, 20 mM; sodium orthovanadate, 2 mM; sodium-pyrophosphate 1 mM; nicotinamide 5 mM; Thiamet G 4 μM and protease inhibitors (SigmaFast, Sigma Aldrich) according to manufacturer's instructions). Equal amounts of protein were separated using SDS-PAGE and transferred to PVDF membranes. Antibodies used for Western blot analyses were: anti-OGT (#SAB2101676 Sigma), anti-O-GlcNAc (#2739 Abcam), anti-ATP synthase β subunit (#A-21351 ThermoFisher Scientific), anti-succinate dehydrogenase A subunit (SDHA) (#14715 Abcam), OGT (#5368 CST), O-GlcNAc (CTD110.6 #9875 CST), OGA (#124807 Abcam), Hexokinase II (#2867 CST), PFK1 (#166722 Santa Cruz Biotechnology (SCBT)), PDH (#C54G1 CST), PDH pS293 (#ABS204 Millipore), PDH pS300 (#ABS194 Millipore), ACC pS79/257 (#07−300 Millipore), Insulin receptor β (#3025 CST), IRS1 (#23822 CST), AKT 1/2/3 (#9272 CST), AKT pT308 (#9275 CST), AKT pS473 (#9271 CST), AKT1 (#5298 SCBT), TBC1D4 (#07−741 Millipore), TBC1D4 pS711 (Custom), TBC1D4 pS324 (Custom), ATGL (#2138 CST), HSL (#4107 CST), HSL pS563 (#4139 CST), GFAT1 (#125069 Abcam), GLUT4 (#PA1-1065 Thermo Fisher).

2.14. Metabolomics analysis

OGT mKO (n = 10) and WT (n = 8) mice underwent a hyperinsulinemic euglycemic clamp. Following this procedure muscle samples were collected, frozen in liquid nitrogen, and stored at −80 °C. Whole muscle sample was pulverized under liquid nitrogen and 30 ± 3 mg (exact mass was noted) underwent metabolomics analysis. Methanol at concentrations 50%, 80%, and 100% with water was used for the metabolites extraction from the muscles. Metabolites were profiled using liquid chromatography combined with mass spectrometry. Following data bucketing and normalization, student t-test with false discovery rate analysis was performed. Detailed metabolomics analysis is available in the Supplementary Materials.

2.15. Quantitative RT-PCR

Directzol RNA Miniprep Kit (Zymo Research) was used to extract total RNA from skeletal muscle or adipose tissue. High-Capacity cDNA Reverse Transcription Kit (Thermo Fisher Scientific) was used to perform reverse transcription. Fast SYBR Green Master Mix (Thermo Fisher Scientific) and 7500 Fast Real Time PCR System (Thermo Fisher Scientific) were used to carry out qPC reaction. Primers used in this paper were published elsewhere [35]. Quantification was performed using ΔΔCT method.

2.16. Muscle extract collection and SVF cell isolation and differentiation

Muscle extracts were collected by isolating both WT and mKO gastrocnemius muscles and placing them in DMEM for 2 h at 37 °C with 80rpm agitation. The conditioned media were collected, and protein concentration determined. The conditioned media were mixed with SVF cell differentiation media to assess the effect of muscle extracts on SVF cell differentiation. For SVF cell isolation, inguinal WATs were collected from adult C57BL/6J mice, minced, and transferred to digestion medium (Ham's F10 medium containing 500 units per mL collagenase II 10% horse serum, 1% penicillin/streptomycin, and 0.1% gentamycin) for 1 h at 37 °C with 80 rpm agitation. To stop the digestion, complete medium (DMEM containing 10% FBS and 1% penicillin/streptomycin) was added followed by triturating 20 times to generate a homogenous mixture. The cells were centrifuged at 450 *g* for 5 min, and the supernatant was discarded. The pellet containing the SVF cells was re-suspended in complete medium, filtered through a 40 μM cell strainer, and the throughput was centrifuged. The pellet was re-suspended in complete medium and plated onto a 15 cm collagen-coated dish. Two hours later the cells were washed with PBS to remove alternate cell types. After reaching confluence, the cells were re-plated on 12-well collagen-coated dishes at 1,000 cells per mm^2. Twenty-four hours after plating, cells were changed to induction medium (complete medium containing 5 μg/μl insulin, 1 nM 3,3′,5-triiodo-L-thyronine, 125 μM indomethacin, 2 μg/mL dexamethasone, and 0.5 mM 3-isobutyl-1-methylxanthine), mixed with WT and mKO muscle extracts in the presence or absence of IL15 antibody. After 72 h the cells were changed to maintenance medium (complete medium containing 5 μg/μL insulin and 1 nM 3,3′,5-triiodo-L-thyronine) with muscle extracts with or without IL15 antibody. After 96 h, the cells were fixed with 10% formalin, stained with Oil Red O, and imaged.

2.17. Immunoprecipitation (IP)

For IP, gastrocnemius muscles were isolated from mice, minced and homogenized in NP40 lysis buffer (50 mM Tris−HCl, 1% NP40, 150 mM NaCl, 1 mM EDTA) in the presence of 1 mM PMSF, 1 μg/mL leupeptin, 1 μg/mL aprotinin, 1 μg/mL pepstatin, 1 mM Na_3VO_4, 1 mM NaF, and 40 μM PUGNAc. Antibodies against O-GlcNAc (Abcam, RL2) and EZH2 (Abcam) were incubated with 500 μg of total protein overnight at 4 °C with agitation, respectively. The immune complexes were incubated with protein A beads, washed, and eluted using sample buffer for further immunoblotting analysis.

2.18. Chromatin immunoprecipitation (ChIP)

ChIP was performed as previously described [36]. The precipitated chromatin was purified and DNA was quantified using quantitative RT-

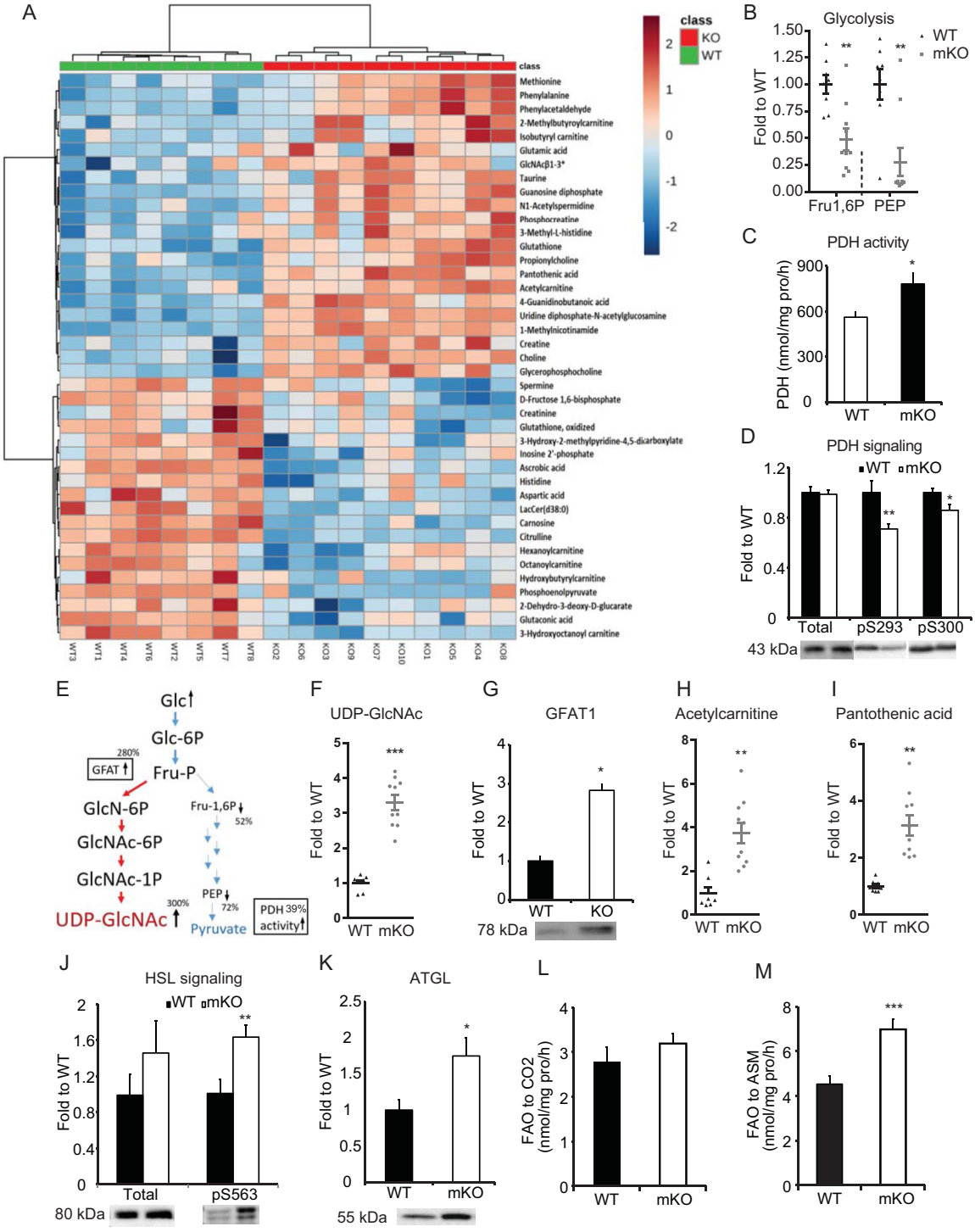

Figure 4: Loss of skeletal muscle OGT alters global muscle metabolism. (A) Metabolome heat map of gastrocnemius muscle from clamped mice. Metabolites were measured using LC-MS. **(B)** Glycolytic metabolites from metabolome. Fructose 1 6-bisphosphate (Fru1,6P) and phosphoenolpyruvate (PEP). **(C)** Pyruvate dehydrogenase (PDH) activity in the gastrocnemius muscle was assayed with the substrate [1−^{14}C] pyruvate by measuring enzyme-catalyzed release of ^{14}CO2. **(D)** Immunoblot of PDH phosphorylation at pS293 and pS300 in gastrocnemius from clamped mice. **(E)** Illustration of metabolites and regulation of glycolysis and hexosamine biosynthetic pathway. **(F)** UDP-GlcNAc levels from the metabolomics analysis. **(G)** Immunoblot of GFAT1 in gastrocnemius from clamped mice. **(H)** Acetylcarnitine levels from the metabolomics analysis. **(I)** Pantothenic acid levels from the metabolomics analysis. **(J)** Immunoblot of HSL and HSL pS563 in gastrocnemius from clamped mice. **(K)** Immunoblot of ATGL in gastrocnemius from clamped mice. **(L)** Complete oxidation of [1−^{14}C]-palmitic acid to CO_2 in gastrocnemius muscle of WT and mKO mice. **(M)** Incomplete oxidation of [1−^{14}C]-palmitic acid to acid-soluble metabolites (ASM) in gastrocnemius muscle. Data represent means ± SEM from n = 8−10, 18-week-old (Panel A, B, C, F, G, H, I, J, and K) and n = 10, 16-week-old (Panel D, L, and M) male mice in each genotype. *p < 0.05; **p < 0.01; ***p < 0.001 compared with WT mice.

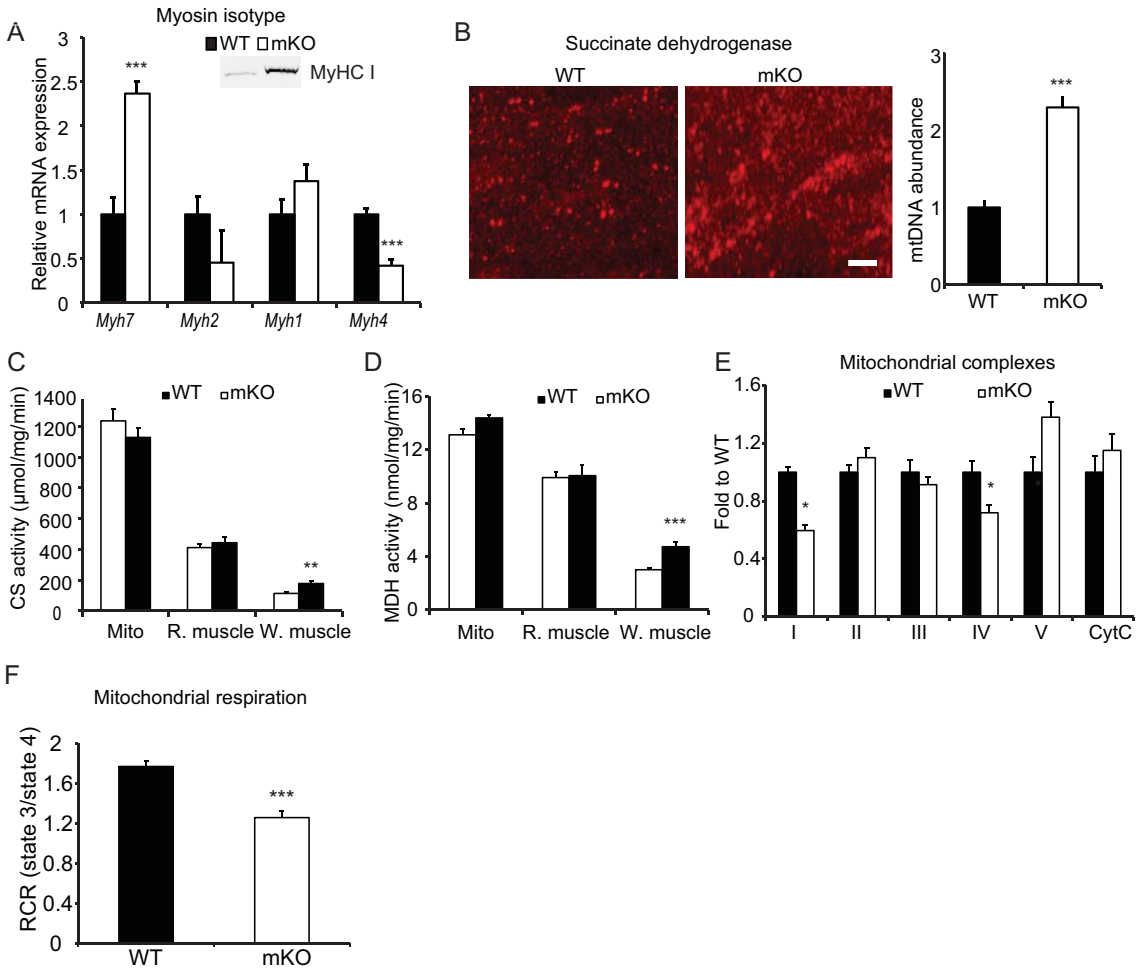

Figure 5: Loss of skeletal muscle OGT increases type I myosin heavy chain-containing fibers, but impairs maximal oxidative capacity. (A) Relative mRNA expression of myosin heavy chain (MyHC) I (*Myh7*), MyHC IIa (*Myh2*), MyHC IIx (*Myh1*), and MyHC IIb (*Myh4*) in the gastrocnemius muscle. Inset, immunoreactivity of MyHC I in the gastrocnemius muscles of WT and mKO muscle. **(B)** Mitochondrial abundance. Left: three-dimensional confocal images showing the difference in mitochondria in gastrocnemius muscle cross-sections of WT and mKO stained with succinate dehydrogenase antibody (left panel). Bar, 5 μm. Right: mitochondrial DNA (mtDNA) abundance in the gastrocnemius muscles of WT and mKO mice. Mt—Co1 DNA was measured using qPCR and normalized to genomic *Nrip1* DNA. **(C—D)** Citrate synthase (CS, C) and malate dehydrogenase (MDH, D) activities in isolated mitochondria (Mito), and red (R.) and white (W.) portions of the gastrocnemius muscles of WT and mKO mice. **(E)** Abundance of mitochondrial complexes in gastrocnemius from clamped mice. **(F)** Mitochondria were isolated from WT and mKO gastrocnemius muscle, and oxygen consumption was measured using Seahorse. Respiration control ratio of state 3/state 4 was calculated based on oxygen consumption rate (OCR) in each state. Data represent means ± SEM from n = 10, 16-week-old male mice in each genotype. *p < 0.05; **p < 0.01; ***p < 0.001 compared with WT mice.

PCR. The ChIP-grade antibodies against O-GlcNAc, EZH2, and H3K27me3 were bought from Abcam. Primers for the *Il15* promoter were as follows: forward GCC TGT TTG GGA ACA GTA AAC; reverse CAA CTT AAA GAT GCT GCC TTA CC.

2.19. Statistical analyses

Results are presented as means ± SEM. Levene's test for homogeneity of variances was performed prior to statistical comparisons between groups. Data were log10 transformed if Levene's test was significant. In all cases, this was sufficient to obtain equal variance. Comparison between two groups was performed using Student's *t* test with two-tailed distribution. For multiple-group comparisons, one-way and two-way ANOVAs were used to test for no differences among the group means. In case of significant interactions, Tukey's multiple comparison test was performed post hoc. $p < 0.05$ was considered statistical significant.

3. RESULTS

3.1. Type 2 diabetes is associated with elevated O-GlcNAcylation levels in skeletal muscle

We hypothesized that increased blood glucose concentrations observed in type 2 diabetic people would result in elevated O-GlcNAcylation of proteins in skeletal muscle. Vastus lateralis muscle biopsies were obtained before and after a 4-hour hyperinsulinemic euglycemic clamp from well-matched lean, obese, and obese, insulin resistant type 2 diabetic patients [25]. We found that 'global' O-GlcNAcylation levels were significantly increased in type 2 diabetic people independent of insulin compared with controls (Figure 1A). Moreover, we quantified protein abundance of key O-GlcNAc-related enzymes OGT, OGA, and glutamine:fructose-6-phosphate amidotransferase (GFAT), all of which showed no difference in total protein abundance (Supplementary Figure 1A—C). These data show that O-

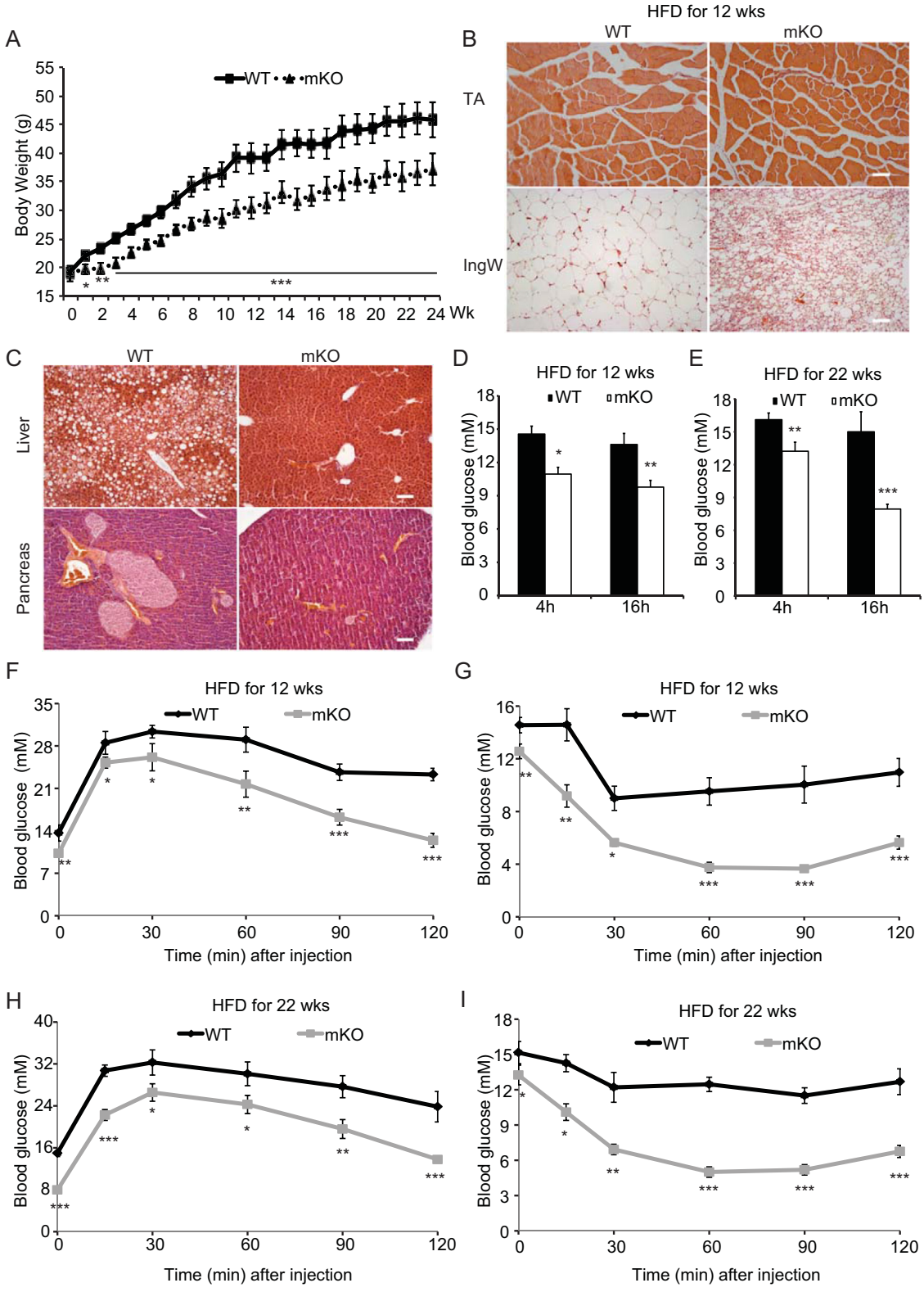

Figure 6: A high-fat diet fail to induce glucose and insulin intolerance in mice lacking muscle OGT. (A) Weekly (Wk) body weights of WT and mKO mice during 24 wks of HFD. HFD feeding started at 4 weeks of age. **(B)** Cross-sections of the tibialis anterior (TA, top row) muscle and inguinal WAT (IngW, bottom row) of WT (left column) and mKO (right column) mice fed HFD for 24 wks. **(C)** Photo micrographs of H&E stained liver (top row) and pancreas (bottom row) sections of WT (left column) and mKO (right column) mice fed HFD for 24 wks. **(D)** Blood glucose levels of WT and mKO mice fed a HFD for 12 wks and fasted for 4 and 16 h, respectively. **(E)** Blood glucose levels in WT and mKO mice fed a HFD for 22 wks and fasted for 4 and 16 h, respectively. **(F–G)** Glucose (F) and insulin (G) tolerance tests of WT and mKO male mice fed a HFD for 12 wks **(H–I)** Glucose (H) and insulin (I) tolerance tests of WT and mKO male mice fed a HFD for 22 wks. Data represent means ± SEM from n = 12 male mice in each genotype. *$p < 0.05$; **$p < 0.01$; ***$p < 0.001$ compared with WT control mice.

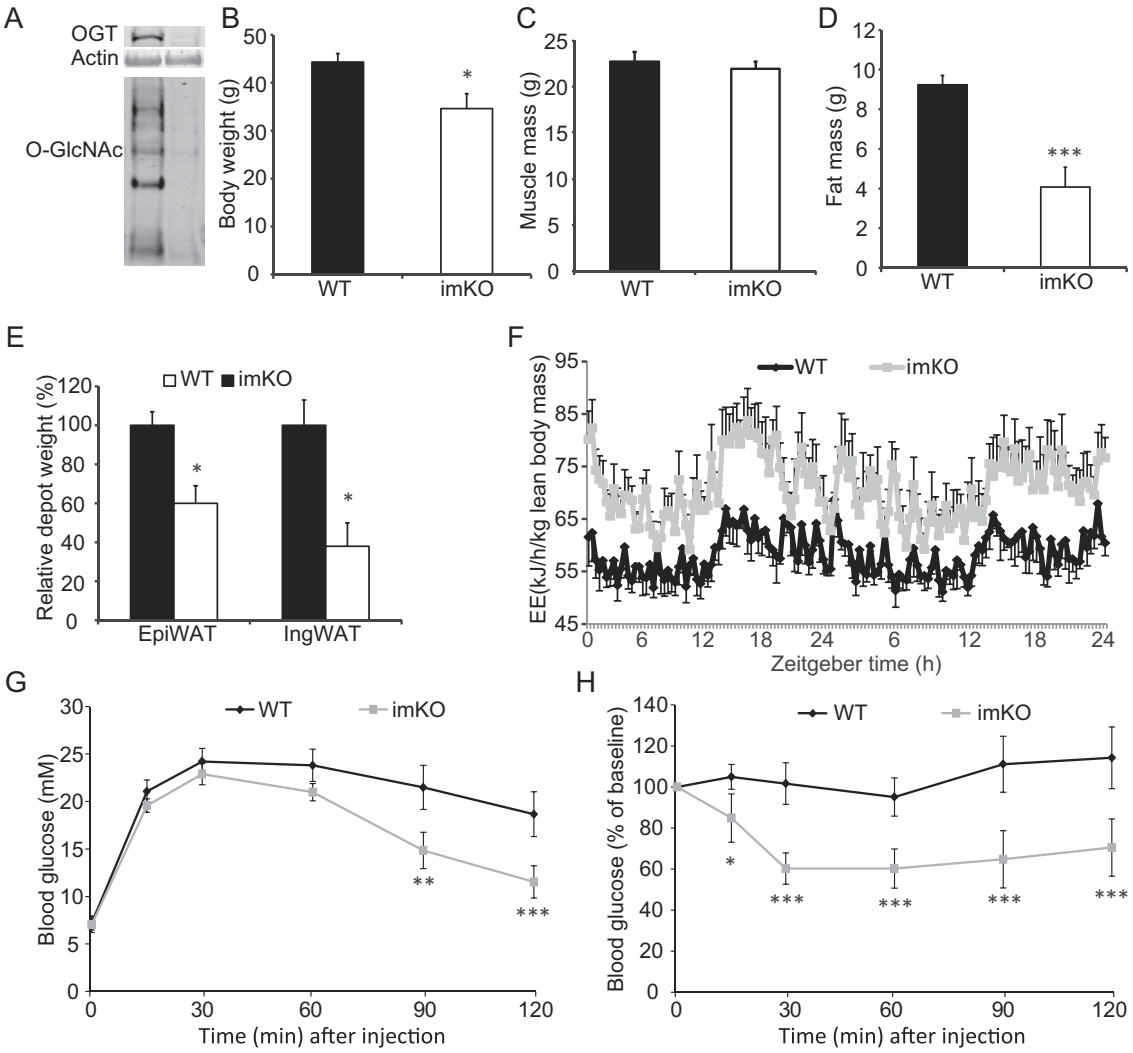

Figure 7: Inducible knockout of OGT in skeletal muscle recapitulates the mKO mouse. OGT knockout was induced when mice were 5 months old by feeding doxycycline food for two weeks. Subsequently, mice were fed normal chow for 6 months before analysis. **(A)** Muscle from WT and imKO mice were immunoblotted with anti-OGT and -O-GlcNAc antibodies respectively. Equal amount of total protein was loaded across all the lanes. **(B–F)** Body weight **(B)**, muscle mass **(C)**, fat mass **(D)**, fat depots **(E)**, and energy expenditure (EE) **(F)** were assessed. **(G–H)** Glucose tolerance test (GTT) **(G)** and insulin tolerance test (ITT) **(H)**. Data represent means ± SEM from n = 10 male mice in each genotype. *p < 0.05; **p < 0.01; ***p < 0.001 compared with WT control mice.

GlcNAcylation increases in muscle tissue with blood glucose levels and suggest that skeletal muscle OGT may be involved in the development of insulin resistance and type 2 diabetes in humans. These data prompted us to investigate further the role of OGT in skeletal muscle.

3.2. Mice lacking muscle OGT have a lean phenotype

To assess the role of OGT in skeletal muscle, we bred male mice harboring Cre recombinase the expression of which was driven by the human skeletal α-actin promoter (HSA-Cre mice) with *Ogt* floxed homozygous female mice to generate muscle-specific hemizygous OGT knockout (mKO) and wild type (WT) mice. OGT was ablated in skeletal muscle as evidenced by the lack of OGT protein in tibialis anterior (TA), soleus, and extensor digitorum longus (EDL) muscle of mKO mice, (Figure 1B). Consequently, O-GlcNAcylation levels in these muscles were greatly reduced (Figure 1C). Moreover, levels of O-GlcNAcase (OGA) were significantly reduced in all three muscles (Figure 1D), suggesting a corresponding compensatory mechanism of the reciprocal cellular O-GlcNAcylation. Additionally, and as expected, we found no difference in OGT protein levels in the heart (Supplementary Figure 2A). By 12 weeks of age, mKO mice had similar body weights compared with WT controls (Figure 1E). However, after 12 weeks of age, mice lacking muscle OGT were significantly smaller than WT mice (Figure 1E), yet no differences in muscle cross sectional area or muscle fiber number were noted in the soleus or EDL muscles (Supplementary Figure 2B–D). This reduction in body mass was associated with a reduction in whole-body fat accumulation (Figure 1F), but not lean mass (Figure 1G) at 16 weeks of age in mKO compared to their WT littermates. Consistently, muscle weights of TA, soleus, and EDL did not differ among genotypes at 16 weeks of age (Figure 1H). Fat depots, including the anterior subcutaneous white adipose tissue (AsW), inguinal white adipose tissue (IngW), and epididymal white adipose tissue (EpiW), but not the brown adipose tissue (BAT), were greatly reduced in mKO compared to those of WT mice (Figure 1I,J). This reduction in fat mass was partly due to smaller adipocytes (Figure 1K) and a corresponding browning of white adipose tissue as assessed by immunohistochemistry analysis for UCP1 (Figure 1L). No differences in *Ucp1* gene expression in BAT were

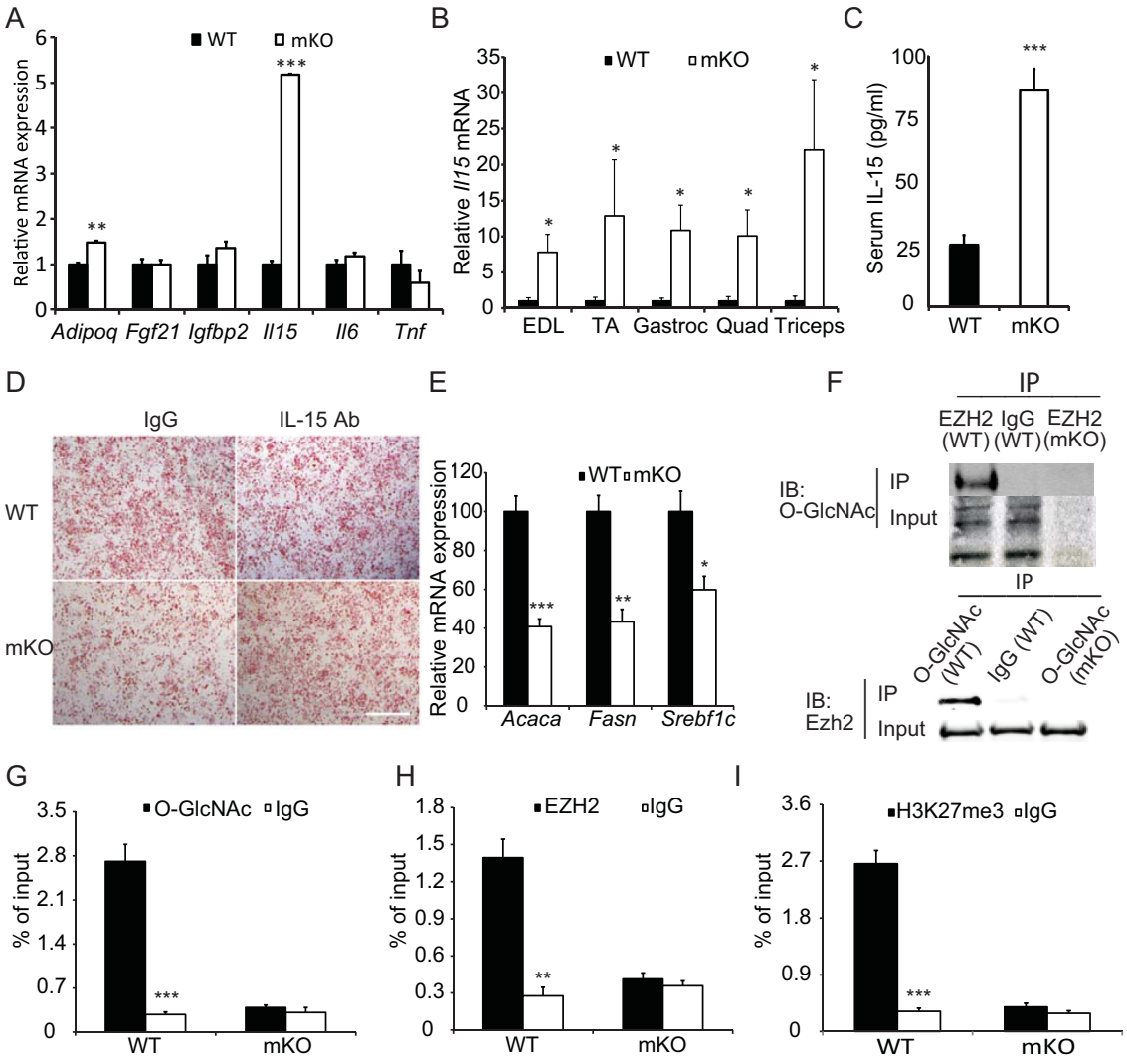

Figure 8: OGT knockout results in augmented Interleukin-15 production in skeletal muscle. (A) Expression of myokines in the gastrocnemius muscles of WT and mKO mice fed HFD for 22 wks **(B)** IL-15 mRNA expression in skeletal muscles from clamped mice (n = 8–10, 18-week-old male mice). **(C)** Serum IL-15 levels in WT and mKO mice fed HFD for 22 wks (n = 10). **(D)** Oil red-O staining of cultured stromal vascular fraction cells isolated from mouse lngW and induced to differentiate in the presence or absence of gastrocnemius muscle extracts from WT (top row) and mKO (bottom row) mice with (right) or without (left) IL15 neutralizing antibodies. Scale bar, 1 mm. **(E)** Expression of lipogenic genes in lngW (n = 10). **(F)** Immunoprecipitation was performed using anti-EZH2 and anti-O-GlcNAc antibodies respectively, and immunoblotted with O-GlcNAc and EZH2 antibodies respectively. **(G–I)** Chromatin immunoprecipitation using antibodies against O-GlcNAc (G), EZH2 (H), and H3K27me3 (I), respectively. Quantitative RT-PCR was used to quantify IL-15 promoter sequence as detailed in Methods. *p < 0.05, **p < 0.01, ***p < 0.001 compared to WT or corresponding antibody-treated samples.

observed (Supplementary Figure 2E). To assess whether muscle function was impacted by OGT ablation, we assessed muscle contractile properties. No differences in single-twitch force (Figure 1M), half-relaxation time of the single twitch (Figure 1N), or time to peak tension (Figure 1O) were observed between WT and mKO EDL muscles. Muscle force of EDL during tetanic contractions increased gradually with stimulation frequency, but no differences were noted between genotypes (Figure 1P). Moreover, we did not observe any differences between WT and mKO soleus and EDL muscles in terms of force production during a single tetanic contraction or fatigue-ability during repeated tetanic contractions (Figure 1Q–T). Collectively, these data show that mKO mice have a lean phenotype due to a reduction in whole-body fat mass, yet no functional alterations in muscle growth, development, or function were identified.

3.3. Muscle-specific ablation of OGT enhances energy expenditure

To investigate the mechanism of the lean phenotype in mice lacking OGT in skeletal muscle, we assessed whole body energy metabolism by indirect calorimetry over a period of 48 h. Interestingly, we found that mKO mice were less active than WT mice in both light and dark phases of the day (Figure 2A,B). While mKO mice had less cage activity, their energy expenditure normalized to lean body mass was greater than WT mice (Figure 2C,D). Additionally, mKO mice had a higher respiratory exchange ratio (RER) compared to WT mice (Figure 2E,F), indicating that these mice have greater reliance on carbohydrates than fat for energy production. Food intake did not differ between genotypes (Figure 2G), but water consumption was greater in the mKO mice (Figure 2H). Given mKO mice weigh less than WT mice from 3 months of age (Figure 1E) and have less cage activity

(Figure 2A,B), we hypothesized that ablation of muscle OGT caused an increase in energy expenditure in the form of heat production. Higher rectal temperatures were indeed noted for mKO mice compared to that of WT mice (Figure 2I). Taken together, these findings suggest that skeletal muscle OGT and O-GlcNAcylation may regulate muscle energy metabolism, which may affect activity and whole body energy balance.

3.4. Lack of OGT in skeletal muscle affects glucose homeostasis, insulin signaling, and whole-body insulin sensitivity

To determine how ablation of OGT in skeletal muscle affects the ability of muscle to handle energy substrates, we performed a hyperinsulinemic euglycemic clamp to assess whole-body insulin sensitivity. Mice were clamped at 6 mM of blood glucose (Figure 3A,B), and mKO mice displayed a profound increase in glucose infusion rate (GIR) (Figure 3C,D). Interestingly, insulin levels at basal and during the clamp were significantly reduced in the mKO compared to WT mice (Figure 3E). We found glucose uptake was markedly increased in TA, gastrocnemius, and triceps from mKO mice compared to WT mice, yet the differences were not consistent among muscles as there was no difference in glucose uptake in the EDL, quadriceps, and soleus muscles between genotypes (Figure 3F). In white adipose tissues, there were noticeable increases in glucose uptake in EpiW and IngW (Figure 3G). In contrast, brown adipose tissue (BAT) displayed a 50% decrease in glucose uptake, and there was no change of glucose uptake in heart or brain (Figure 3H). Glycogen levels in the liver after the clamp was increased in mKO mice, but skeletal muscle glycogen levels were not different between genotypes (Figure 3I). However, liver glycogen of the non-insulin-stimulated mKO cohort, used as blood donors for the clamped mice, was also increased (Figure 3J). While our data suggest that skeletal muscle and white adipose tissue are mainly responsible for the enhanced GIR in the mKO mice, the liver may play an important role in whole-body glucose utilization in these mice. In clamped gastrocnemius muscle, in which glucose uptake was increased, both total Akt protein abundance and Akt phosphorylation at T308 and S473 were increased in mKO mice compared to WT littermates (Figure 3K). Total Akt1 protein levels did not differ between genotypes (Figure 3L), suggesting that the enhanced level of Akt in the mKO mice is due to increased Akt2 abundance. Interestingly, the difference in Akt signaling between genotypes was not associated with differences in TBC1D4 phosphorylation status (Figure 3M); however, GLUT4 levels were significantly increased in the gastrocnemius muscle of the mKO mice compared to WT mice (Figure 3N). These data suggest that differences observed in whole body insulin sensitivity may not be due to classical insulin signaling events in skeletal muscle but may still be mediated by a larger increase in GLUT4 at the plasma membrane at a given insulin concentration.

3.5. Loss of OGT alters global muscle metabolism

Because loss of OGT in skeletal muscle resulted in increased energy expenditure and whole-body insulin sensitivity, we explored metabolic changes in skeletal muscle that could explain the lean phenotype of mKO mice. To this end, we investigated muscle metabolite levels in the gastrocnemius of clamped mice. Using an LC/MS-based metabolomics analysis, we identified 41 metabolites that differed between genotypes (Figure 4A). Of these, fructose 1,6 biphosphate (Fru-1,6P) and phosphoenolpyruvate (PEP) were reduced by 52% and 72%, respectively, in mKO muscle compared to WT muscle (Figure 4B). Western blot analyses revealed that hexokinase II (HKII) and phosphofructokinase 1 (PFK1) protein levels were unchanged (Supplementary Figure 2F,G). However, basal activity of pyruvate dehydrogenase (PDH) in non-insulin-stimulated gastrocnemius muscle was enhanced in mKO mice compared to WT mice (Figure 4C), and phosphorylation of PDH at S293 and S300 was decreased in clamped gastrocnemius muscle from mKO mice compared to WT mice (Figure 4D). These results indicate that, in response to insulin, glycolytic flux downstream of PEP is increased or that glucose is shunted into other pathways upstream of Fru-1,6P. The level of UDP-GlcNAc was upregulated by more than 300% in mKO (Figure 4E,F) compared to WT mice, and this increase was accompanied by a 3-fold upregulation of GFAT, which is the rate-limiting enzyme in the hexosamine biosynthesis pathway (HBP) (Figure 4G). Together, our data suggest that mKO muscle upregulates activities of both glycolysis and the HBP at least in clamped mice. However, the importance of the two pathways for glucose disposal in basal or clamp settings cannot be quantitatively evaluated using the available data.

Apart from changes in intracellular glucose metabolism, the metabolomics analysis indicated changes in fatty acid oxidation. Acetyl carnitine level (Figure 4H) was upregulated several fold in mKO mice compared to WT mice, so was the CoA precursor pantothenic acid (Figure 4I), indicating that mKO mice exhibited increased capacity to shuttle fatty acids from the cytosol into the mitochondria. This was supported by the finding of increased *Cpt1α* and *Cpt1β* mRNA expression (Supplementary Figure 2H), although only *Cpt1α* levels were significantly changed. In addition, we found the total level of hormone sensitive lipase (HSL) to be unaltered, but HSL phosphorylation at S563, a surrogate measure of HSL activity, was significantly increased in mKO mice compared to WT mice (Figure 4J). Furthermore, adipose triglyceride lipase (ATGL) protein level was upregulated by 1.75 fold in mKO mice (Figure 4K). To assess whether beta-oxidation was altered, we measured fatty acid oxidation (FAO) in unstimulated gastrocnemius muscle. Interestingly, while there was no difference in complete fatty acid oxidation between WT and mKO muscles (Figure 4L), mKO muscles contained a significantly higher level of acid-soluble metabolites (ASM) (Figure 4M), a hallmark of incomplete FAO. However, mRNA levels of genes involved in FAO (i.e., *Acadl* and *Acadm*) were not significantly changed (Supplementary Figure 2H). Together, these data indicate that mKO muscle attempts to increase fatty acid oxidation, but increased ASMs suggest that complete oxidation of fatty acids may be impaired in skeletal muscle of these mice.

3.6. OGT ablation alters muscle oxidative capacity

In general, slow-twitch myofibers are enriched with mitochondria, capillaries and myoglobin, and they predominately use oxidative phosphorylation for ATP production. Fast-twitch myofibers, on the other hand, are more glycolytic and deposit greater amounts of glycogen as an energy reserve [37–39]. To test whether OGT ablation causes changes in muscle fiber type composition, and thus oxidative capacity, we measured the expression of myosin heavy chain (MyHC) I (*Myh7*), IIa (*Myh2*), IIx (*Myh1*), and IIb (*Myh4*) genes in the gastrocnemius muscle. Type I MyHC gene expression was significantly upregulated and type IIb MyHC gene expression was downregulated in OGT ablated muscle (Figure 5A). Consistent with increases in *Myh7* expression, the corresponding protein levels were also elevated in OGT mKO muscles (Figure 5A, inset). Moreover, three-dimensional confocal microscopy revealed that mKO muscle contains more mitochondria compared to WT muscle (Figure 5B), and increased mitochondrial content was confirmed by an increased mitochondrial DNA to nuclear DNA ratio in the gastrocnemius muscle (Figure 5B). Citrate synthase and malate dehydrogenase activity were also higher in white part of

the gastrocnemius muscle from mKO mice (Figure 5C,D). However, when we measured the abundance of specific proteins in the OXPHOS complexes, we found complex V to be increased (although not significantly), whereas complex I and IV were reduced significantly in mKO compared to WT muscle (Figure 5E). To test the function of the mitochondria, we isolated mitochondria from gastrocnemius muscle and measured oxygen consumption rates. We found that mitochondria from mKO muscle have compromised respiration control ratio of state 3/state 4, indicating dysfunctional mitochondria (Figure 5F). Taken together, we show that dysregulation of O-GlcNAcylation in skeletal muscle drives muscle to a slower contracting, oxidative phenotype but perhaps at the expense of properly functional mitochondria.

3.7. High-fat diets fail to induce insulin resistance in mice lacking muscle OGT

Because mice lacking OGT in skeletal muscle are leaner, have higher energy expenditure, and are more insulin sensitive than WT mice, we challenged these mice with a high-fat diet (HFD) and monitored glucose metabolism and insulin action. WT mice fed a HFD for 24 weeks gained significantly more weight than the HFD-fed mKO mice (Figure 6A). At the end of HFD feeding, no differences in skeletal muscle fiber size were found, whereas the lngW of mKO mice exhibited significant browning compared with that of WT mice (Figure 6B). In lngW, mRNA expression of genes involved in browning was also significantly upregulated (Supplementary Figure 2I). In the liver of WT mice lipid accumulation was wide-spread, whereas very little was detected in the mKO mice (Figure 6C). Moreover, hypertrophy of pancreatic islets was evident in the WT mice but no such obesity-induced pathology was noted in mKO mice (Figure 6C). Consistently, blood glucose levels after a 4-h fast in mKO mice fed 12 (Figure 6D) or 22 (Figure 6E) weeks of HFD were significantly lower than in WT controls. In addition, after 22 weeks on the HFD, blood glucose levels of WT mice did not respond to 16 h of fasting, but decreased even further in the mKO mice compared with the 4 h fast (Figure 6E). Results from glucose and insulin tolerance tests (Figure 6F—I) showing improved glycemic control in the mKO mice, further support the notion that dysregulation of skeletal muscle OGT may modulate obesity-related phenotypes in other tissues to regulate whole body insulin sensitivity.

3.8. Inducible ablation of OGT in skeletal muscle recapitulates the mKO mouse

To exclude the possibility that the aforementioned observations were simply a consequence of OGT-mediated defects early in development, we generated inducible muscle-specific OGT KO (imKO) mice by crossing floxed OGT mice with tetracycline/doxycycline inducible HSA-cre mouse. Five-month-old adult mice were fed chow containing doxycycline for two weeks to induce knockout of OGT in skeletal muscle. Approximately six months after OGT ablation, we evaluated mice with regard to muscle and fat masses, energy expenditure, and insulin tolerance. Western blot analyses using anti-OGT and O-GlcNAc antibodies confirmed OGT ablation in skeletal muscle (Figure 7A). imKO mice had reduced body weights after OGT ablation (Figure 7B). Similar to mKO mice, imKO mice had normal muscle mass (Figure 7C), reduced fat mass (Figure 7D,E) and enhanced energy expenditure (Figure 7F). Furthermore, imKO mice were more insulin responsive than their WT counterparts, as evidenced by glucose (Figure 7G) and insulin (Figure 7H) tolerance tests, respectively. These data show ablation of OGT in adult skeletal muscle recapitulates the OGT mKO phenotype suggesting that suppression of O-GlcNAc signaling in skeletal muscle of adult mice promotes an increase in whole body energy metabolism and reduces adiposity.

3.9. OGT ablation results in augmented skeletal muscle Interleukin-15 production

To determine how muscle-specific knockout of OGT affects adipose tissue, we analyzed a panel of myokines that are known to exert local and systemic effects on adipose tissue function. Of the six myokines selected, only *Il15* and *Adipoq* was significantly up-regulated in mKO muscle (Figure 8A,B). Because circulating IL-15 has well-documented anti-obesity effects [40], we analyzed serum IL-15 levels and found that circulating IL-15 concentrations in mKO mice were consistently 2.5-fold higher than WT mice (Figure 8C). To investigate a potential connection between elevated IL-15 and reduced fat mass, we used an *in vitro* cell culture system in which stromal vascular fraction (SVF) cells were cultured with muscle extracts from either WT or mKO mice to evaluate the effect on lipid accumulation. Extracts from mKO muscle inhibited SVF cell differentiation as evidenced by less lipid droplet formation (Oil-Red-O staining) compared with muscle extracts from WT mice (Figure 8D). However, this inhibition was released when an IL-15-neutralizing antibody was introduced into the media (Figure 8D). Furthermore, quantitative RT-PCR of the lipogenic genes revealed that *Acaca, Fasn, and Srebf1c* were significantly reduced in mKO muscle extract-treated SVF cells (Figure 8E). These results show that muscle from mice lacking a functional OGT in muscle produce greater levels of circulating IL-15 that may affect adipose tissue development and function. Our data also suggest that OGT may be directly involved in regulating *Il15* gene expression in skeletal muscle.

At the molecular level, OGT has been shown to repress gene expression epigenetically. It was shown that O-GlcNAcylation stabilizes histone methyltransferase enhancer of zeste homolog 2 (EZH2), which facilitates the formation of the trimethylation of histone 3 at lysine 27 (H3K27me3) thereby repressing gene expression in human MCF-7 cells [41]. To explore the possible existence of a similar mechanism in skeletal muscle, we used co-immunoprecipitation (Co-IP) to study the interaction of OGT and EZH2. Co-IP results revealed that OGT can O-GlcNAcylate EZH2 in skeletal muscle (Figure 8F). To assess whether the OGT and EZH2 interaction has any relevance to *Il15* gene regulation, we conducted a chromatin immunoprecipitation (ChIP) assay. O-GlcNAc, EZH2, and H3K27me3 were all enriched at the *Il15* promoter region (Figure 8G—I). These findings suggest the existence of the OGT-EZH2-H3K27me3 axis in skeletal muscle, similar to the mechanism responsible for controlling gene repression in a human adenocarcinoma cell line. These results indicate that the increases in circulating IL-15 we observed in mKO mice are likely mediated by epigenetic regulation of the *Il15* gene locus.

4. DISCUSSION

Despite its discovery three decades ago, the physiological significance of O-GlcNAcylation as a nutrient sensor has only recently been recognized [42]. O-GlcNAc is a dynamic posttranslational modification that is targeted to Ser/Thr residues by O-GlcNAc transferase (OGT) and removed by O-GlcNAcase (OGA). The substrate for OGT is UDP-GlcNAc, a product of the hexosamine biosynthetic pathway (HBP). UDP-GlcNAc is an ideal gauge of metabolic status because levels reflect fluxes through a number of metabolic pathways, especially carbohydrate metabolism. Based on our finding that O-GlcNAcylation levels were elevated in skeletal muscle from T2D people, we hypothesized that OGT may be important for nutrient sensing in this tissue and for whole body insulin sensitivity. Data presented herein clearly demonstrate that skeletal muscle OGT is centrally important for maintaining muscle energy homeostasis, mitochondrial function, and insulin sentivity. Moreover, we show that *Il15* gene transcription is epigenetically

controlled by OGT. Thus, given the role of IL-15 in exogenous lipid partitioning [43], OGT in skeletal muscle is important not only for the ability to survey cellular nutrient status but also for regulation of substrate availability.

OGT mKO mice were markedly more insulin sensitive compared with WT controls. *In vivo* studies involving manipulation of the HBP support this finding. Mice that transgenically overexpress GFAT in GLUT4 expressing tissues show an opposite phenotype with decreased whole body insulin sensitivity measured using the hyperinsulinimic euglycemic clamp technique [44]. Likewise, if OGT is overexpressed using a similar approach, whole body insulin sensitivity is also decreased, and mice display hyperinsulinemia [22]. Thus, manipulation of flux through the HBP appears to affect insulin action, and the HBP could serve as a potential pharmacological target. Interestingly, not all muscle types from the OGT mKO mice showed enhanced glucose uptake in response to insulin compared with WT littermates. We have only analyzed the gastrocnemius muscle from the clamp experiment; therefore, we are not currently able to explain these muscle type differences. However, it was recently shown that IL-15 activates the JAK3/STAT3 pathway in skeletal muscle cells, and this induces glucose uptake [45]. Therefore, we speculate that the responsiveness to IL-15 may be different between muscle types in OGT mKO mice. Further studies are necessary to address this intriguing observation.

Based on PDH activity and the level of glycolytic intermediates in the gastrocnemius muscle in response to insulin, knockout of OGT appears to alter glycolytic flux. Overexpression of OGT in SY5Y cells decreases glycolysis [46], and several proteins within the glycolytic pathway are known to be O-GlcNAcylated in rat skeletal muscle [47] and in HEK293 cells [48]. Thus, our data are in line with the idea that OGT may act as a mediator of this pathway. Moreover, since manipulation of O-GlcNAc signaling affects mitochondrial function and dynamics in cardiac myocytes [49], in muscle cells *in vitro* [50], and in skeletal muscle (the present study), it is conceivable that changes in glycolytic flux can be explained in part by changes in the capacity or efficiency for ATP generation by oxidative phosphorylation.

Lack of discernable histological and functional anomalies in skeletal muscle of OGT mKO mice argues that OGT may not be requisite for normal muscle function. This is somewhat surprising given the widely abundant nature of O-GlcNAcylation on structural muscle proteins [1]. However, the idea that O-GlcNAcylation is a part of a complex nutrient-sensing pathway, whereby protein O-GlcNAcylation serves as a niche-based nutrient sentinel for cells, remains intriguing especially from a whole organismal vantage point. Indeed, surveying nutrient availability is important in times of both nutrient plenty and scarcity. Nutrient availability is one of the most effective means of controlling epigenetic events [10]. We show that *Il15* expression is a consequence of OGT ablation in skeletal muscle. Specifically, we observed nearly a 5-fold increase in skeletal muscle *Il15* mRNA expression, which resulted in a corresponding increase in circulating levels of IL-15 in mKO mice. Given that O-GlcNAcylation parallels nutrient availability in cells [51,52] and that chromatin is a major site of O-GlcNAcylation [53–56], we hypothesized that OGT plays a role in the epigenetic regulation of *Il15* gene expression [10,57]. Indeed, OGT O-GlcNAcylates EZH2, a key part of the polycomb repressive complex 2 (PRC2), which may repress *Il15* expression through H3K27me3 modifications [10]. Using co-immunoprecipitation and chromatin immunoprecipitation assays, we found that OGT, EZH2, and H3K27me3 localize to *Il15* promoter sequences and that the increase in muscle-specific IL-15 production is, in part, due to epigenetic modification of the promoter. Moreover, our data are clearly in line with the repressive effect of OGT on *Il15* expression in muscle. We cannot exclude the possibility that OGT ablation results in other yet unknown skeletal muscle permutation(s) that may directly or indirectly disrupt other cellular pathways that increase muscle energy expenditure and lead to a leaner phenotype. Nor can we rule out other molecular 'insults' that may drive increases in cytokine production [58] in our KO mice. Even so, muscle-derived IL-15 production increases in response to a whole-body energy imbalance [59] and may in part explain a number of the characteristics displayed in mice lacking effective O-GlcNAc signaling events in skeletal muscle.

IL15 is highly expressed in human skeletal muscle tissue compared to most other tissues of the body [60] suggesting a critical role for the growth and maintenance of skeletal muscle. Recent studies show that IL-15 have little effect on skeletal muscle accretion [61,62] and raise the possibility that IL-15 acts as a means to elicit responses in distal whole body repositories as a means of mobilizing energy substrates to support its needs. Indeed, IL-15 is now known as a myokine that targets remote tissues to liberate energy resources [63]. Furthermore, prolonged stimulation of muscle by IL-15 increases *Ppargc1a*, *Sirt1*, and *Ucp2* expression, all highly indicative of the conversion of skeletal muscle to a more oxidative phenotype [64]. Congruent with this, OGT mKO mice were indeed more oxidative than WT mice as evidenced by greater mitochondrial DNA and enzyme contents and greater amounts of type I myosin heavy chain isoform. These data argue that OGT mKO mice have greater capacity to oxidize energy substrates, which is in line with calorimetry estimates showing that these mice exhibit greater energy expenditure regardless of the time-of-day studied.

Despite many similarities between the *Il15* transgenic model [64] and the OGT mKO model, they differ on key aspects. OGT mKO mice were more sedentary than controls, which differs from mice over-expressing *Il15* [64]. Whether the increase in body temperature affects the desire to move or whether loss of OGT in tissues somehow keeps animals from moving requires additional attention. Even so, both models show increases in markers indicative of enhanced oxidative capacity. Despite this, OGT mKO mice have higher utilization of glucose relative to fatty acids as evidenced by the higher RER. Increased energy expenditure in combination with impaired mitochondrial function may account for this phenotype, and our current thinking is that lack of OGT may increase oxidative capacity but may also result in mitochondrial insults rendering the mitochondrial machinery impaired.

Mice lacking functional OGT were smaller than their WT littermates. However, this reduction in weight was not due to decreased muscle mass but rather a 50% reduction in adipose tissue weight. Curiously, mice receiving exogenous IL-15 experience similar reductions in whole-body adiposity without reductions in food intake [65–67]. This is also observed in rats administered recombinant IL-15 and mice overexpressing an *Il15* transgene [62,64,68]. Conversely, those mice lacking a functional *Il15* gene are obese [69]. Fat cells of OGT mKO mice were also smaller suggesting OGT ablation in skeletal muscle altered lipogenesis and lipolysis in adipose tissue, two well-known IL-15 functions [66,70]. Additionally, inguinal white adipose tissue contained greater levels of UCP1 protein and many browning marker genes were also upregulated. These data suggest up-regulation of muscle IL-15 in response to OGT ablation in skeletal muscle may be responsible for a leaner phenotype, perhaps by partitioning substrates away from adipose tissue and/or increasing energy expenditure in skeletal muscle. To address this thesis further, we subjected mKO mice to a high-fat diet to induce obesity [71]. As expected, over-fed mKO mice were leaner and had improved blood glucose levels compared to WT controls suggesting ablation of OGT in skeletal muscle altered whole body glucose tolerance. These findings supported our thesis, as those mice over-expressing IL-15 are also protected from this type of induced obesity [62]. Even so, however, discrepancies

between *Il15* overexpressing mice and OGT mKO mice are not surprising given the magnitude of increases observed in overexpressing models and the fact that OGT ablation likely impacts the function of many cytosolic, nuclear, and mitochondrial proteins [48].

In preparation of this manuscript, two studies were published on the role of OGT in skeletal muscle using skeletal muscle-specific OGT KO mice. In one study, no differences in glucose metabolism were observed between OGT KO and WT [72]. However, animals used were 10–12 weeks of age, and, as our data show that the phenotype of muscle-specific OGT KO mice develops from 12 weeks of age, we believe that the authors simply missed the phenotype of the mice in that study. This was confirmed in a follow-up study performed by the same authors in which muscle-specific OGT KO mice were studied at older age [73]. In that study, the observed phenotype of the OGT KO mice corroborated our findings of enhanced energy expenditure, improved whole body insulin sensitivity, and the resistance to obesity in response to HFD feeding.

In summary, results of the present study demonstrate a role of OGT in the maintenance of skeletal muscle energy metabolism and whole-body metabolic homeostasis. Lack of OGT results in increased whole body energy expenditure, altered muscle substrate utilization, and loss in the ability of muscle cells to regulate *Il15* expression. Consequences of increased plasma IL-15 levels likely include changes in the ability to store and metabolize energy substrates, which improves whole-body insulin sensitivity and enhances resistance to obesity. From an evolutionary viewpoint, it makes sense for animals to have a mechanism in place that regulates partitioning of substrates from energy stores. For instance, during fasting, flux through the HBP would be reduced. Consequently, UDP-GlcNAc levels would be lowered, which would result in diminished OGT activity. In turn, the inhibitory effects on *Il15* expression would be released, allowing an elevation in circulating levels of IL-15, which would promote mobilization of lipids from adipose depots. Further studies are needed to fully understand how other whole body and tissue-specific functions are impacted by OGT ablation in muscle. Moreover, additional work is required to dissect more precisely the differences observed between mKO mice and models in which circulating IL-15 levels are elevated.

AUTHOR CONTRIBUTIONS

HS, AM, JTT, and DEG designed the experiments. HS, AM, TSN, MRD, LL, SL, KF, HWG, KS, RK, TF, MMA, ZS, and UKH conducted experiments and analyzed the data. EME, ZC, MWH, and RFH provided expertise for data interpretation. JFPW and KH performed the human experiments. XY provided founder OGT KO mice. HS, AM, JTT, and DEG wrote the manuscript. All authors read and approved the final version of the paper. JTT and DEG secured funding and provided supervision.

ACKNOWLEDGEMENTS

The authors would like to thank Prof. Thomas Mandrup-Poulsen, University of Copenhagen, and Dr. LeBris S. Quinn for constructive comments during the manuscript preparation. Support for this study was provided by the Novo Nordisk Foundation Center for Basic Metabolic Research. The Novo Nordisk Foundation Center for Basic Metabolic Research is an independent Research Center at the University of Copenhagen that is partially funded by an unrestricted donation from the Novo Nordisk Foundation, http://metabol.ku.dk). JTT was supported by the Novo Nordisk Foundation (Excellence Project Award; NNF14OC0009315), by the Danish Council for Independent Research (Research Project Grant; DFF-4004-00235), and by the European Foundation for the Study of Diabetes (EFSD/Lilly Research Fellowship). JFPW was supported by the Novo Nordisk Foundation (NNF 160C0023046) and The Danish Medical Research Council (DFF-6110-00498B).

CONFLICT OF INTEREST

None declared.

APPENDIX A. SUPPLEMENTARY DATA

Supplementary data related to this article can be found at https://doi.org/10.1016/j.molmet.2018.02.010.

REFERENCES

[1] Bond, M.R., Hanover, J.A., 2013. O-GlcNAc cycling: a link between metabolism and chronic disease. Annual Review of Nutrition 33:205–229.
[2] Slawson, C., Copeland, R.J., Hart, G.W., 2010. O-GlcNAc signaling: a metabolic link between diabetes and cancer? Trends in Biochemical Sciences 35:547–555.
[3] Issad, T., Masson, E., Pagesy, P., 2010. O-GlcNAc modification, insulin signaling and diabetic complications. Diabetes & Metabolism 36:423–435.
[4] Lefebvre, T., Dehennaut, V., Guinez, C., Olivier, S., Drougat, L., Mir, A.M., et al., 2010. Dysregulation of the nutrient/stress sensor O-GlcNAcylation is involved in the etiology of cardiovascular disorders, type-2 diabetes and Alzheimer's disease. Biochimica Et Biophysica Acta (BBA)-General Subjects 1800:67–79.
[5] Ruan, H.B., Singh, J.P., Li, M.D., Wu, J., Yang, X., 2013. Cracking the O-GlcNAc code in metabolism. Trends in Endocrinology and Metabolism 24:301–309.
[6] Bullen, J.W., Balsbaugh, J.L., Chanda, D., Shabanowitz, J., Hunt, D.F., Neumann, D., et al., 2014. Cross-talk between two essential nutrient-sensitive enzymes: O-GlcNAc transferase (OGT) and AMP-activated protein kinase (AMPK). Journal of Biological Chemistry 289:10592–10606.
[7] Xu, J., Wang, S., Viollet, B., Zou, M.H., 2012. Regulation of the proteasome by AMPK in endothelial cells: the role of O-GlcNAc transferase (OGT). PLoS One 7:e36717.
[8] Ruan, H.B., Han, X., Li, M.D., Singh, J.P., Qian, K., Azarhoush, S., et al., 2012. O-GlcNAc transferase/host cell factor C1 complex regulates gluconeogenesis by modulating PGC-1alpha stability. Cell Metabolism 16:226–237.
[9] Xu, X.J., Valentine, R.J., Ruderman, N.B., 2014. AMP-activated protein kinase (AMPK): does this master regulator of cellular energy state distinguish insulin sensitive from insulin resistant obesity? Current obesity reports 3:248–255.
[10] Hanover, J.A., Krause, M.W., Love, D.C., 2012. Bittersweet memories: linking metabolism to epigenetics through O-GlcNAcylation. Nature Reviews Molecular Cell Biology 13:312–321.
[11] Harwood, K.R., Hanover, J.A., 2014. Nutrient-driven O-GlcNAc cycling - think globally but act locally. Journal of Cell Science 127:1857–1867.
[12] Lagerlof, O., Slocomb, J.E., Hong, I., Aponte, Y., Blackshaw, S., Hart, G.W., et al., 2016. The nutrient sensor OGT in PVN neurons regulates feeding. Science 351:1293–1296.
[13] Ruan, H.B., Dietrich, M.O., Liu, Z.W., Zimmer, M.R., Li, M.D., Singh, J.P., et al., 2014. O-GlcNAc transferase enables AgRP neurons to suppress browning of white fat. Cell 159:306–317.
[14] Bostrom, P., Wu, J., Jedrychowski, M.P., Korde, A., Ye, L., Lo, J.C., et al., 2012. A PGC1-alpha-dependent myokine that drives brown-fat-like development of white fat and thermogenesis. Nature 481:463–468.
[15] Funai, K., Song, H., Yin, L., Lodhi, I.J., Wei, X., Yoshino, J., et al., 2013. Muscle lipogenesis balances insulin sensitivity and strength through calcium signaling. Journal of Clinical Investigation 123:1229–1240.
[16] Song, R., Peng, W., Zhang, Y., Lv, F., Wu, H.K., Guo, J., et al., 2013. Central role of E3 ubiquitin ligase MG53 in insulin resistance and metabolic disorders. Nature 494:375–379.

[17] Watt, M.J., Dzamko, N., Thomas, W.G., Rose-John, S., Ernst, M., Carling, D., et al., 2006. CNTF reverses obesity-induced insulin resistance by activating skeletal muscle AMPK. Natura Med 12:541—548.
[18] Baskin, K.K., Winders, B.R., Olson, E.N., 2015. Muscle as a "mediator" of systemic metabolism. Cell Metabolism 21:237—248.
[19] Hardie, D.G., Schaffer, B.E., Brunet, A., 2016. AMPK: an energy-sensing pathway with multiple inputs and outputs. Trends in Cell Biology 26:190—201.
[20] Ross, F.A., MacKintosh, C., Hardie, D.G., 2016. AMP-activated protein kinase: a cellular energy sensor that comes in 12 flavours. FEBS Journal 283:2987—3001.
[21] Love, D.C., Hanover, J.A., 2005. The hexosamine signaling pathway: deciphering the "O-GlcNAc code". Science's STKE 2005:re13.
[22] McClain, D.A., Lubas, W.A., Cooksey, R.C., Hazel, M., Parker, G.J., Love, D.C., et al., 2002. Altered glycan-dependent signaling induces insulin resistance and hyperleptinemia. Proceedings of the National Academy of Sciences of the United States of America 99:10695—10699.
[23] Huang, P., Ho, S.R., Wang, K., Roessler, B.C., Zhang, F., Hu, Y., et al., 2011. Muscle-specific overexpression of NCOATGK, splice variant of O-GlcNAcase, induces skeletal muscle atrophy. American Journal of Physiology - Cell Physiology 300:C456—C465.
[24] Ogawa, M., Mizofuchi, H., Kobayashi, Y., Tsuzuki, G., Yamamoto, M., Wada, S., et al., 2012. Terminal differentiation program of skeletal myogenesis is negatively regulated by O-GlcNAc glycosylation. Biochimica et Biophysica Acta (BBA)-General Subjects 1820:24—32.
[25] Hojlund, K., Birk, J.B., Klein, D.K., Levin, K., Rose, A.J., Hansen, B.F., et al., 2009. Dysregulation of glycogen synthase COOH- and NH2-terminal phosphorylation by insulin in obesity and type 2 diabetes mellitus. The Journal of Cinical Endocrinology and Metabolism 94:4547—4556.
[26] Birk, J.B., Wojtaszewski, J.F., 2006. Predominant alpha2/beta2/gamma3 AMPK activation during exercise in human skeletal muscle. Journal of Physiology 577:1021—1032.
[27] Wolff, A.V., Niday, A.K., Voelker, K.A., Call, J.A., Evans, N.P., Granata, K.P., et al., 2006. Passive mechanical properties of maturing extensor digitorum longus are not affected by lack of dystrophin. Muscle & Nerve 34:304—312.
[28] Treebak, J.T., Birk, J.B., Hansen, B.F., Olsen, G.S., Wojtaszewski, J.F., 2009. A-769662 activates AMPK beta1-containing complexes but induces glucose uptake through a PI3-kinase-dependent pathway in mouse skeletal muscle. American Journal of Physiology-Cell Physiology 297: C1041—C1052.
[29] Jensen, B.A., Nielsen, T.S., Fritzen, A.M., Holm, J.B., Fjaere, E., Serup, A.K., et al., 2016. Dietary fat drives whole-body insulin resistance and promotes intestinal inflammation independent of body weight gain. Metabolism 65: 1706—1719.
[30] Ayala, J.E., Bracy, D.P., McGuinness, O.P., Wasserman, D.H., 2006. Considerations in the design of hyperinsulinemic-euglycemic clamps in the conscious mouse. Diabetes 55:390—397.
[31] Ferre, P., Leturque, A., Burnol, A.F., Penicaud, L., Girard, J., 1985. A method to quantify glucose utilization in vivo in skeletal muscle and white adipose tissue of the anaesthetized rat. The Biochemical Journal 228:103—110.
[32] Frezza, C., Cipolat, S., Scorrano, L., 2007. Organelle isolation: functional mitochondria from mouse liver, muscle and cultured fibroblasts. Nature Protocols 2:287—295.
[33] Gerencser, A.A., Neilson, A., Choi, S.W., Edman, U., Yadava, N., Oh, R.J., et al., 2009. Quantitative microplate-based respirometry with correction for oxygen diffusion. Analytical Chemistry 81:6868—6878.
[34] Frisard, M.I., McMillan, R.P., Marchand, J., Wahlberg, K.A., Wu, Y., Voelker, K.A., et al., 2010. Toll-like receptor 4 modulates skeletal muscle substrate metabolism. American Journal of Physiology. Endocrinology and Metabolism 298:E988—E998.
[35] Kim, K.H., Jeong, Y.T., Oh, H., Kim, S.H., Cho, J.M., Kim, Y.N., et al., 2013. Autophagy deficiency leads to protection from obesity and insulin resistance by inducing Fgf21 as a mitokine. Natura Med 19:83—92.
[36] Nelson, J.D., Denisenko, O., Bomsztyk, K., 2006. Protocol for the fast chromatin immunoprecipitation (ChIP) method. Nature Protocols 1:179—185.
[37] Bassel-Duby, R., Olson, E.N., 2006. Signaling pathways in skeletal muscle remodeling. Annual Review of Biochemistry 75:19—37.
[38] Gunning, P., Hardeman, E., 1991. Multiple mechanisms regulate muscle fiber diversity. The FASEB Journal 5:3064—3070.
[39] Richard, A.F., Demignon, J., Sakakibara, I., Pujol, J., Favier, M., Strochlic, L., et al., 2011. Genesis of muscle fiber-type diversity during mouse embryogenesis relies on Six1 and Six4 gene expression. Developmental Biology 359: 303—320.
[40] Ye, J., 2015. Beneficial metabolic activities of inflammatory cytokine interleukin 15 in obesity and type 2 diabetes. Frontiers of Medicine 9: 139—145.
[41] Chu, C.S., Lo, P.W., Yeh, Y.H., Hsu, P.H., Peng, S.H., Teng, Y.C., et al., 2014. O-GlcNAcylation regulates EZH2 protein stability and function. Proceedings of the National Academy of Sciences of the United States of America 111:1355—1360.
[42] Hart, G.W., 2014. Three decades of Research on O-GlcNAcylation - a major nutrient sensor that regulates signaling, transcription and cellular metabolism. Frontiers in Endocrinology (Lausanne) 5:183.
[43] Duan, Y., Li, F., Wang, W., Guo, Q., Wen, C., Li, Y., et al., 2017. Interleukin-15 in obesity and metabolic dysfunction: current understanding and future perspectives. Obesity Reviews 18:1147—1158.
[44] Cooksey, R.C., Hebert Jr., L.F., Zhu, J.H., Wofford, P., Garvey, W.T., McClain, D.A., 1999. Mechanism of hexosamine-induced insulin resistance in transgenic mice overexpressing glutamine:fructose-6-phosphate amidotransferase: decreased glucose transporter GLUT4 translocation and reversal by treatment with thiazolidinedione. Endocrinology 140:1151—1157.
[45] Krolopp, J.E., Thornton, S.M., Abbott, M.J., 2016. IL-15 activates the Jak3/STAT3 signaling pathway to mediate glucose uptake in skeletal muscle cells. Frontiers in Physiology 7:626.
[46] Tan, E.P., Villar, M.T., E, L., Lu, J., Selfridge, J.E., Artigues, A., et al., 2014. Altering O-linked beta-N-acetylglucosamine cycling disrupts mitochondrial function. Journal of Biological Chemistry 289:14719—14730.
[47] Cieniewski-Bernard, C., Bastide, B., Lefebvre, T., Lemoine, J., Mounier, Y., Michalski, J.C., 2004. Identification of O-linked N-acetylglucosamine proteins in rat skeletal muscle using two-dimensional gel electrophoresis and mass spectrometry. Molecular & Cellular Proteomics 3:577—585.
[48] Hahne, H., Sobotzki, N., Nyberg, T., Helm, D., Borodkin, V.S., van Aalten, D.M., et al., 2013. Proteome wide purification and identification of O-GlcNAc-modified proteins using click chemistry and mass spectrometry. Journal of Proteome Research 12:927—936.
[49] Gawlowski, T., Suarez, J., Scott, B., Torres-Gonzalez, M., Wang, H., Schwappacher, R., et al., 2012. Modulation of dynamin-related protein 1 (DRP1) function by increased O-linked-beta-N-acetylglucosamine modification (O-GlcNAc) in cardiac myocytes. Journal of Biological Chemistry 287:30024—30034.
[50] Wang, X., Feng, Z., Wang, X., Yang, L., Han, S., Cao, K., et al., 2016. O-GlcNAcase deficiency suppresses skeletal myogenesis and insulin sensitivity in mice through the modulation of mitochondrial homeostasis. Diabetologia 59: 1287—1296.
[51] Arias, E.B., Kim, J., Cartee, G.D., 2004. Prolonged incubation in PUGNAc results in increased protein O-Linked glycosylation and insulin resistance in rat skeletal muscle. Diabetes 53:921—930.
[52] Yang, W.H., Park, S.Y., Nam, H.W., Kim, D.H., Kang, J.G., Kang, E.S., et al., 2008. NFkappaB activation is associated with its O-GlcNAcylation state under hyperglycemic conditions. Proceedings of the National Academy of Sciences of the United States of America 105:17345—17350.
[53] Fujiki, R., Hashiba, W., Sekine, H., Yokoyama, A., Chikanishi, T., Ito, S., et al., 2011. GlcNAcylation of histone H2B facilitates its monoubiquitination. Nature 480:557—560.

[54] Ozcan, S., Andrali, S.S., Cantrell, J.E., 2010. Modulation of transcription factor function by O-GlcNAc modification. Biochimica et Biophysica Acta (BBA)-Gene Regulatory Mechanisms 1799:353—364.

[55] Sakabe, K., Hart, G.W., 2010. O-GlcNAc transferase regulates mitotic chromatin dynamics. Journal of Biological Chemistry 285:34460—34468.

[56] Zhang, S., Roche, K., Nasheuer, H.P., Lowndes, N.F., 2011. Modification of histones by sugar beta-N-acetylglucosamine (GlcNAc) occurs on multiple residues, including histone H3 serine 10, and is cell cycle-regulated. Journal of Biological Chemistry 286:37483—37495.

[57] Lewis, B.A., Hanover, J.A., 2014. O-GlcNAc and the epigenetic regulation of gene expression. Journal of Biological Chemistry 289:34440—34448.

[58] Rinnov, A., Yfanti, C., Nielsen, S., Akerstrom, T.C., Peijs, L., Zankari, A., et al., 2014. Endurance training enhances skeletal muscle interleukin-15 in human male subjects. Endocrine 45:271—278.

[59] Gleeson, M., 2000. Interleukins and exercise. Journal of Physiology 529(Pt 1):1.

[60] Grabstein, K.H., Eisenman, J., Shanebeck, K., Rauch, C., Srinivasan, S., Fungl, V., et al., 1994. Cloning of a T cell growth factor that interacts with the beta chain of the interleukin-2 receptor. Science 264:965—968.

[61] Pistilli, E.E., Quinn, L.S., 2013. From anabolic to oxidative: reconsidering the roles of IL-15 and IL-15Ralpha in skeletal muscle. Exercise and Sport Sciences Reviews 41:100—106.

[62] Quinn, L.S., Anderson, B.G., Strait-Bodey, L., Stroud, A.M., Argiles, J.M., 2009. Oversecretion of interleukin-15 from skeletal muscle reduces adiposity. American Journal of Physiology. Endocrinology and Metabolism 296:E191—E202.

[63] Pedersen, B.K., Akerstrom, T.C., Nielsen, A.R., Fischer, C.P., 2007. Role of myokines in exercise and metabolism. Journal of Applied Physiology 103: 1093—1098 (1985).

[64] Quinn, L.S., Anderson, B.G., Conner, J.D., Wolden-Hanson, T., 2013. IL-15 overexpression promotes endurance, oxidative energy metabolism, and muscle PPARdelta, SIRT1, PGC-1alpha, and PGC-1beta expression in male mice. Endocrinology 154:232—245.

[65] Alvarez, B., Carbo, N., Lopez-Soriano, J., Drivdahl, R.H., Busquets, S., Lopez-Soriano, F.J., et al., 2002. Effects of interleukin-15 (IL-15) on adipose tissue mass in rodent obesity models: evidence for direct IL-15 action on adipose tissue. Biochimica et Biophysica Acta (BBA)-General Subjects 1570:33—37.

[66] Carbo, N., Lopez-Soriano, J., Costelli, P., Alvarez, B., Busquets, S., Baccino, F.M., et al., 2001. Interleukin-15 mediates reciprocal regulation of adipose and muscle mass: a potential role in body weight control. Biochimica et Biophysica Acta (BBA)-General Subjects 1526:17—24.

[67] Carbo, N., Lopez-Soriano, J., Costelli, P., Busquets, S., Alvarez, B., Baccino, F.M., et al., 2000. Interleukin-15 antagonizes muscle protein waste in tumour-bearing rats. British Journal of Cancer 83:526—531.

[68] Almendro, V., Busquets, S., Ametller, E., Carbo, N., Figueras, M., Fuster, G., et al., 2006. Effects of interleukin-15 on lipid oxidation: disposal of an oral [(14)C]-triolein load. Biochimica et Biophysica Acta (BBA)-Molecular and Cell Biology of Lipids 1761:37—42.

[69] Barra, N.G., Reid, S., MacKenzie, R., Werstuck, G., Trigatti, B.L., Richards, C., et al., 2010. Interleukin-15 contributes to the regulation of murine adipose tissue and human adipocytes. Obesity (Silver Spring) 18:1601—1607.

[70] Ajuwon, K.M., Spurlock, M.E., 2004. Direct regulation of lipolysis by interleukin-15 in primary pig adipocytes. American Journal of Physiology-Regulatory, Integrative and Comparative Physiology 287:R608—R611.

[71] Surwit, R.S., Kuhn, C.M., Cochrane, C., McCubbin, J.A., Feinglos, M.N., 1988. Diet-induced type II diabetes in C57BL/6J mice. Diabetes 37:1163—1167.

[72] Ida, S., Morino, K., Sekine, O., Ohashi, N., Kume, S., Chano, T., et al., 2017. Diverse metabolic effects of O-GlcNAcylation in the pancreas but limited effects in insulin-sensitive organs in mice. Diabetologia 60:1761—1769.

[73] Murata, K., Morino, K., Ida, S., Ohashi, N., Lemecha, M., Park, S.Y., et al., 2018. Lack of O-GlcNAcylation enhances exercise-dependent glucose utilization potentially through AMP-activated protein kinase activation in skeletal muscle. Biochemical and Biophysical Research Communications 495:2098—2104.

